Multiphysics microfluidics for cell manipulation and separation: a review

ccMultiphysics Microfluidics for Cell Manipulation and Separation: A Review

Haotian Cha[1], Hedieh Fallahi[1], Yuchen Dai[1], Dan Yuan[2], Hongjie An[1], Nam-Trung Nguyen[1]*, Jun Zhang[1]*

[1] Queensland Micro- and Nanotechnology Centre, Griffith University, Nathan, Queensland 4111, Australia. E-mail: jun.zhang@griffith.edu.au; nam-trung.nguyen@griffith.edu.au

[2] Centre for Regional and Rural Futures, Deakin University, Geelong, Victoria 3216, Australia

Abstract

Multiphysics microfluidics, which combines multiple functional physics in a microfluidic platform, is an emerging research area that attracts increasing interest in diverse biomedical applications. Multiphysics microfluidics is expected to overcome the limitations of individual physical phenomena by combining their advantages. Furthermore, multiphysics microfluidics is superior for cell manipulation due to the high precision, better sensitivity and real-time tunability, and multi-targets sorting capability. These exciting features motivate us to review the state of the art of this field and reassess the feasibility of multiple physical coupling. To confine the scope of this paper, we mainly focus on five common forces in microfluidics: inertial lift, elastic, dielectrophoresis (DEP), magnetophoresis (MP) and acoustic forces. This review first explains the working mechanisms based on single physics. Next, we classify multiphysics techniques as cascaded connection and physical coupling, and elaborate the combination of design and working mechanism of the systems reported in the literature to date. Finally, we discuss the possibility and design scheme of combining multiple physics and propose several promising future directions.

Keywords: Multiphysics microfluidics/ Cascaded connection/ Physical coupling/ Inertial/ Elastic/ DEP/ Magnetic/ Acoustic/ Cell manipulation and separation

1 Introduction

Cell manipulation and separation are essential for applications in biomedical research,[1] clinical diagnosis,[2] drug discovery,[3] and tissue engineering [4] etc. Microfluidics is an emerging platform technology that processes or manipulates fluids and analytes in channels from tens to hundreds of micrometres.[5] Microfluidics offers the unparalleled capability for precise manipulation and separation of cells even at a single-cell level because the characteristic scale of microfluidic structures matches that of cells.

Effective manipulating concepts are needed to control the motion of cells in microchannels precisely. Generally, microfluidic techniques can be categorized as active and passive techniques according to the sources of the manipulating forces. Active techniques rely on external sources such as electric, [6-9] magnetic,[10, 11] acoustic,[12-14] optical,[15-20] and thermal [21-24] fields. On the contrary, passive technology works based on inherent channel geometry, fluid rheology, and fluid dynamics. Passive techniques include microfilters,[25-27] pinched flow fractionation (PFF),[28-30] deterministic lateral displacement (DLD),[31-33] inertial microfluidics [34-36] and viscoelastic microfluidics.[37-39] Each manipulation technique has its advantages and limitations. In general, active methods are excellent in precisely controlling cells through adjusting external force fields in real-time. However, the flow speed has to be generally slow for the drag force to match in the order of magnitude with manipulating forces acting on the target cells, thus limiting the throughput. In contrast, passive techniques are ordinarily simple, easy to operate, and generally have a higher throughput. However, passive techniques lack real-time controllability and onsite flexibility. Moreover, the accuracy of passive techniques is relatively lower compared to the active counterparts. Both active and passive techniques have been extensively utilized for manipulation and separation of cells and particles such as blood cells,[40, 41] cancer cells,[42, 43] algae,[44, 45] bacteria,[46, 47] yeast,[48] virus,[49, 50] and extracellular vesicles,[51, 52] etc.

A single microfluidic technique cannot always provide a satisfactory outcome for real-world complex and heterogeneous samples, where cell properties (such as size, density, shape, and deformability, etc.) of different cells often overlap, making separation difficult. For instance, the size overlap of circulating tumour cells (CTCs) and blood cells compromised size-based microfluidic separation techniques.[2, 53] Therefore, a combination of two or more techniques is needed. In the last decade, a growing number of works reports the integration of two or more techniques in one device for processing complex samples.[54-56] The combination can be in the formats of cascaded connection [57-59] or physical coupling.[56, 60, 61] Cascaded

connection is a “serial circuit” in which fluids and particles continuously pass through working sections with a particular separation technique. In each section, a particular physical force is in charge of particle manipulation. Physical coupling is similar to a “parallel circuit”, where multiple manipulation forces apply on the particles simultaneously. In the former format, each section is relatively independent, and the manipulating physics applies to the cells individually and do not interact with each other. The only connection between the sections is the fluid flow. In the latter format, multiple physics are coupled through the forces acting on the same fluid particle. The superposition or balance of these forces determines the motion and equilibrium location of the particles. In addition, the interaction between these physical fields may also occur, consequently altering the resulting manipulation force. Delicate coupling of multiple physics may enable more precise control of cells and better functionalities. However, this manipulation concept is still underexplored due to the complexity of multiphysics phenomena.

As an emerging field, combinatory multiphysics microfluidics has been attracting increasing interest from the research community. This paper reviews the state of the art of the field, evaluates possible combinations of physical phenomena and proposes basic feasible design schemes. This review paper is organized as follows. We first explain the working mechanisms of the various single-physics phenomena. Next, we review the current development of combining multiple physics phenomena by cascaded connection and physical coupling. We elaborate on the design and working mechanism of the reported systems. Finally, we discuss the basic design schemes for multiphysics microfluidics and provide a perspective on future research and application directions.

2 Physics of manipulating forces

In this section, we summarize the physics and mechanism of each manipulation type in microfluidics. To keep the scope of this paper within a reasonable breath, we do not exhaustively list all the manipulation force types, but mainly focus on five main forces, i.e., inertial lift force, elastic force, dielectrophoresis (DEP), magnetophoresis (MP), and acoustic force. We do not include other manipulating forces such as optical and thermophoresis because their relatively small magnitude and not commonly used in continuous-flow microfluidics.

2.1 Drag force

Drag force is not a manipulating force that can be adjusted to control, but a passive force induced by the relative motion of particles and fluid. A relative motion between particles and the fluid elements always occurs when an external manipulating force moves the particles

across the fluid streamline. The relative motion induces a drag force on the particle, Figure 1(A). Therefore, the balance of drag force and applied force determines the final relative velocity of particles to the fluid. According to the Stokes law, the drag force applied on a moving spherical particle is:[35]

$$F_{drag} = 3\pi\mu a v_t \quad (1)$$

where v_t=v_f-v_p is the relative velocity of the fluid to the particle. In the following discussion, we exclude drag force as an effective manipulating force, because this force is intrinsically induced when there is a relative motion between particles and fluids, and its primary role is to balance other induced forces.

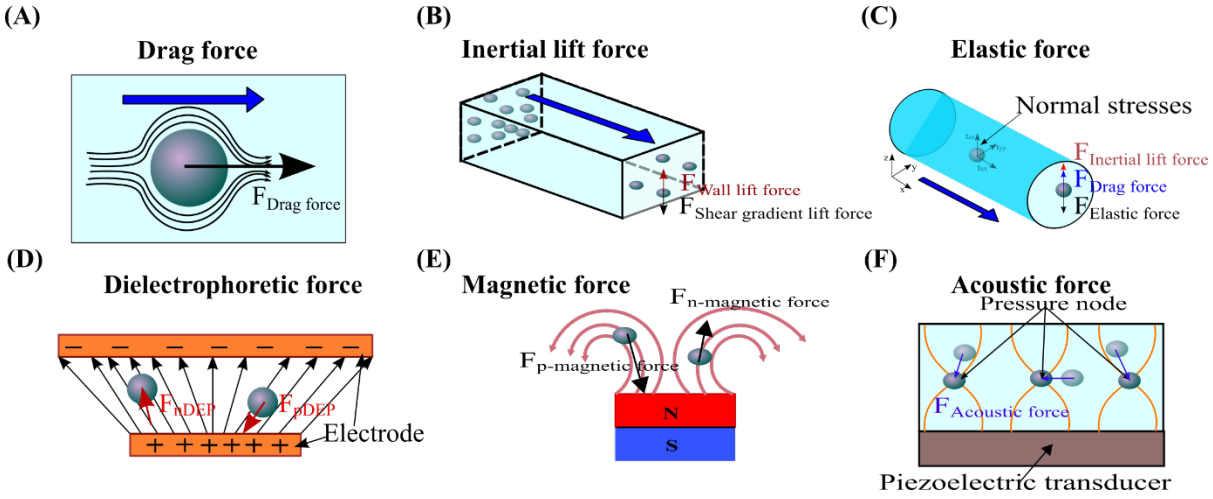

2.2 Inertial lift forces

The inertial lift forces arise due to the finite inertia of fluid flow in the intermediate Reynolds number range (~1<Re<~100, Re $= \frac{\rho U D_h}{\mu}$, with ρ the fluid density, U the average flow velocity, μ the dynamic viscosity, and D_h the hydraulic diameter [62]) between Stokes flow (Re<<1) and turbulent flow.[35, 63] The inertial lift forces move a particle to equilibrium positions within the microchannel. The balance between the shear gradient lift force F_{LS} and the wall lift force F_{LW} determines the equilibrium positions in straight microchannels,[35, 64] Figure 1(B). The shear gradient lift force F_{LS} is caused by the parabolic velocity profile and its interaction with the particle. The wall lift force F_{LW} is induced by the disturbance from the surrounding flow field of a particle and its reflection off the wall [60]. The net inertial lift force can be described as:[65]

$$F_L = \frac{\rho U^2 a^4}{{D_h}^2} f_L(Re, z), \quad (2)$$

where, f_L is the lift coefficient, which is related to the position of z-direction and Reynold number; and a is the particle diameter. To date, various microchannel types have been utilised for inertial microfluidics, including straight,[66, 67] spiral,[68-71] serpentine,[72, 73] expansion-contraction [74-76] channels and their combination.[57, 60, 77] Inertial lift forces have been utlised successfully in biomedical applications such as isolation of circulating tumour cells (CTCs),[78-81] separation of blood cells,[40, 82, 83] solution exchange,[84, 85] separation of malaria pathogen,[75, 86] sorting of algae cells,[87, 88] cell cycle synchronization,[89] cell encapsulation [90] etc.

2.3 Elastic force

Viscoelastic fluids, which mainly consist of non-Newtonian fluids with elasticity and non-constant viscosity in response to the rate of strain, manipulate particles by an elastic force.[91] The elastic force results from the non-uniform normal stress mismatch of a non-Newtonian viscoelastic fluid flow.[92-94] The first normal stress difference $N_1=\tau_{xx}-\tau_{yy}$ and the second normal stress difference $N_2=\tau_{yy}-\tau_{zz}$ determine the elastic force.[95] The first normal stress N_1 applies an extra tension along with the main flow, whereas the second normal stress N_2 induces a secondary flow within the channel cross-section. Here, τ_{xx}, τ_{yy} and τ_{zz} are stresses along the main flow, velocity gradient and vorticity direction, respectively.[96] In a diluted viscoelastic polymer solution, the strength of N_2 is much smaller than N_1. Therefore, the second normal stress N_2 can be neglected.[96, 97] Thus, the elastic lift force is proportional to the variation of N_1 over the particle size and can be expressed as:

$$F_e = C_{eL} a^3 \nabla N_1 = -2 C_{eL} a^3 \eta_p \lambda \nabla \dot{\gamma}^2, \quad (3)$$

$$N_1 = -2\eta_p \lambda \dot{\gamma}^2, \quad (4)$$

where C_{eL} is the non-dimensional elastic lift coefficient and η_p is the polymeric contribution of the solution viscosity; λ is the relaxation time and $\dot{\gamma}$ is the average shear rate, which can be expressed as $\dot{\gamma} = \frac{2U}{D_h}$.[97] The elastic force focuses particles into the low shear rate region, such as the centreline of a circular channel, Figure 1(C). Weissenberg number or Deborah number is used to characterise the viscoelastic effect, defined as the ratio of the fluid relaxation time to the characteristic time (t_f) of fluid flow:[91]

$$Wi = \frac{\lambda}{t_f} = \lambda \dot{\gamma} = \lambda \frac{2U}{D_h} \quad (5)$$

Furthermore, as both the inertial and elastic effects may be significant, the elasticity number (EL) characterizes the ratio of the elastic force to inertial force:[38]

$$EL = \frac{\mathrm{Wi}}{\mathrm{Re}} = \frac{2\lambda u}{\rho {D_h}^2} \tag{6}$$

Viscoelastic fluids for particle and cell focusing include both biological fluids (such as DNA [98-100] and hyaluronic acid (HA) solutions [101]) and synthetic aqueous solutions [102] (such as polyvinylpyrrolidone (PVP),[103] polyethylene oxide (PEO),[104] and polyacrylamide (PAA) [105, 106]). The elastic force has been successfully utilized to focus and align cells,[107] solution exchange,[108, 109] cell separation,[97, 110, 111] cell stretching,[112] exosome isolation,[113, 114] and DNA concentration [100, 115] etc.

2.4 Dielectrophoretic (DEP) force

In a spatially uniform electric field, dispersed particles will migrate in the fluid, and this motion is defined as electrophoresis (EP) [Micromachines 2016, 7, 195]. The EP mobility of particles depends on the particle charge and the properties of electric double layer among the particles and electrolyte [J. Fluid Mech. (2019), vol. 874, pp. 856–890]. On the contrary, Dielectrophoresis (DEP) refers to the translational motion of particles within a non-uniform electric field, Figure 1(D). The DEP force is induced by the interaction of a field-induced electrical polarisation with the non-uniform electrical field [116]. Under an alternating electrical field, the time-averaged DEP force is expressed as:[117, 118]

$$F_{Dep} = 2\pi\varepsilon_m r^3 Re[K(\omega)]\nabla|E_{rms}|^2 \tag{7}$$

where, ε_m is the permittivity of the suspending medium; r presents the radius of a spherical particle; E_{rms} is the root-mean-squared value of the applied electrical field; Re $[K(\omega)]$ is the real part of the Clausius–Mossotti (CM) factor. The CM factor is defined as:[116, 119]

$$K(\omega) = \frac{{\varepsilon_p}^* - {\varepsilon_m}^*}{{\varepsilon_p}^* + 2{\varepsilon_m}^*}, \tag{8}$$

$${\varepsilon_p}^* = \varepsilon_p - \frac{i\sigma_p}{\omega}, \tag{9}$$

$${\varepsilon_m}^* = \varepsilon_m - \frac{i\sigma_m}{\omega}, \tag{10}$$

where, ${\varepsilon_p}^*$ and ${\varepsilon_m}^*$ are the complex permittivity of the particle and medium, respectively. ε_p, σ_p and σ_m are the permittivity and conductivity of particle, and conductivity of the medium, respectively. ω is the angular frequency of the electric field.

Furthermore, if the applied electrical field is direct current (DC), the frequency of the electric field is zero, and the CM factor can be simplified as:[116, 119]

$$f_{CM,DC} = \frac{\sigma_p - \sigma_m}{\sigma_p + 2\sigma_m} \tag{11}$$

If the CM factor is positive, where the permittivity or conductivity of particle is greater than that of the medium, the positive DEP (p-DEP) force attracts particles to the region with a higher electric field. However, if the polarization of cells is lower than that of the medium, the CM factor is negative. The negative DEP (n-DEP) force repels particles to the area with a low electric field.[120-122] A non-uniform electric field is critical for DEP. The two main types of DEP devices reported in the literature are electrode-based and insulator-based devices.[123] Electrode-based devices utilized 2D and 3D conducting microelectrode structures to induce a non-uniform electric field.[124-134] In contrast, insulator-based DEP devices employ insulating structures such as obstacles [135, 136] and curved channels [137, 138] to generate an electric field gradient.[139-141] DEP forces can be used to manipulate particles such as DNA,[142] protein,[143] virus,[144, 145] bacteria,[146, 147] blood cells,[148, 149] cancer cells [125, 150, 151] etc.

2.5 Magnetic force

Magnetofluidics utilizes magnetic force for handling fluids and particles in microfluidics.[152] Magnetophoresis, which is the movement of particles in a magnetic field, is one of the most conventional methods for manipulating cells.[153] This non-destructive method can selectively control the migration of target particles/cells based on their magnetic properties.[154] For a uniformly magnetized bead, the magnetic force is:[155]

$$F_{mag} = \frac{V_p * \Delta\chi}{\mu_0} (\mathrm{B} \cdot \nabla)\mathrm{B}, \tag{12}$$

where, V_p presents the volume of the particle. $\Delta\chi = \chi_\mathrm{p} - \chi_\mathrm{f}$ the difference in magnetic susceptibilities of the particle and the base fluid. The term $(\mathrm{B}\cdot\nabla)\cdot\mathrm{B}$ represents the magnetic force field, μ_0 is the permeability of the vacuum. Therefore, the relative difference of magnetic susceptibilities between the particle and the solution determines the direction of the particle migration. If the particle is attracted to the maximum of the magnetic field ($\Delta\chi > 0$), the effect is called positive magnetophoresis. In contrast, if the particle is repelled from the maximum of the field ($\Delta\chi < 0$), the effect is negative magnetophoresis,[156] Figure 1(E). Magnetophoresis provides a broad range of applications, including blood cells separation,[157-159] CTCs

isolation,[160-163] stem cells purification,[164, 165] bacteria trapping and detection,[166-168] 3D cell manipulation,[169, 170] and tissue engineering [156, 171] etc.

2.6 Acoustic forces

Acoustofluidics utilizes an acoustic field to manipulate fluids and particles. The migration of particles in an acoustic field is called acoustophoresis (AP). The acoustic radiation force or the pressure node manipulate particles/cells in space and time.[12, 14] Bulk acoustic waves (BAWs) and surface acoustic waves (SAWs) are the two common waves used in acoustofludiics.[172-174] The magnitude of the acoustic radiation force on spherical particles can be described as:[175, 176]

$$F_R = -\left(\frac{\pi {P_0}^2 V_\mathrm{p} \beta_\mathrm{f}}{2\lambda}\right) \phi(\beta, \rho) \sin(2kx) \tag{13}$$

$$\phi(\beta, \rho) = \frac{5\rho_\mathrm{P} - 2\rho_\mathrm{f}}{2\rho_\mathrm{P} + \rho_\mathrm{f}} - \frac{\beta_\mathrm{p}}{\beta_\mathrm{f}} \tag{14}$$

where, P_0 is the acoustic pressure. β and ρ represent compressibility and density, respectively. Subscript f and p represent fluid and particle, respectively. λ_w and x are wavelength and distance from a pressure node, respectively. ϕ represents the acoustic contrast factor, and it determines the acoustic force direction. The negative acoustic force ($\phi > 0$) attracts particles to the pressure nodes; however, the positive acoustic force ($\phi < 0$) repels the particles to stay away from the pressure nodes (anti-nodes),[177] Figure 1(F).

Acoustic manipulation is label-free and has shown excellent biocompatibility, which is feasible and versatile for separation,[178-180] focusing,[181-183] trapping,[184, 185] enrichment [186, 187] and patterning [188, 189] of various biological particles, such as blood cells,[190, 191] CTCs,[153, 192] bacteria,[193, 194] extracellular vesicles,[195, 196] lipoproteins [197] and DNA.[198, 199]

2.7 Comparison of manipulating forces

The above sections describe the fundamentals and applications of single-physics phenomena for particle manipulation. We summarize and compare the mechanism, advantages, and limitations of these single-physics phenomena in Table 1. Microfluidic techniques based on a single manipulation force type have shown remarkable progress.[200-202] However, for real-world complex and heterogeneous samples, a single manipulation type or a single processing step cannot always meet the separation need. Therefore, a combination of two or more manipulation techniques is emerging as a promising approach. In the following sections, we will elaborate on the current development of combinatory strategies based on cascaded connection and physical coupling in a microfluidic platform. The outline of multiphysics microfluidics is

shown in Figure 2. We will also describe the motivation of integration, device functionality, and applications for each integrated device.

Table 1. Summary of advantages and disadvantages of different single force situation

Physic	Working Mechanism	Source	Advantages	Limitations	Reference
Inertial	Interaction of parabolic fluid velocity and disturbance of channel walls with particles	High flow speed (~10<Re<~100)	High throughput, simple structure, label-free, high biocompatibility	Dilution of samples, fixed geometry, lack of tuneable control, deficient separation resolution	35, 63, 203
Viscoelastic	Non-uniform normal stress differences across particles	Viscoelastic fluid flow (Blood, polymer solution)	3D particle focusing, simple channel structure, micro- and nano scale bioparticles manipulation	Polymer molecules side effect, low Reynolds number, adhesion, or slip at the solid/liquid boundaries	37, 91, 105
DEP	Interaction of electrical polarisation of particles with the non-uniform electrical field	AC and DC electrical field; Metal electrodes or insulator structures	High selectivity and sensitivity, precise manipulation, label-free applications, real-time control, automation, compatible with both microfluidics and electronics	Joule heating effect, low to medium throughput, limited regions of DEP force, side effect on the viability of cells, bulky and complex operating system	8, 123, 139, 204
Magnetic	Homogeneous/inhomogeneous magnetic field	Magnetic source (Permanent magnetic, electromagnets, ferromagnetic wire)	High purity, high specificity isolation of cells based on magnetic labelling, or label-free manipulation of cells based on negative magnetophoresis	The extra cost of magnetic markers, relatively low throughput	11, 154, 205, 206

Acoustic	Acoustic radiation pressure transfers the momentum from the acoustic wave to the particle	Ultrasonic transducer, interdigitated transducers (IDTs)	Wide operation range in channel spatially, contact-free manipulation, wide versatility, biocompatibility, high precision, tuneable control, flexible functions	Induced thermal energy increases temperature, relatively low throughput, issues of wavelength and diffraction, imprecise control in z-axis, expensive electronic system	[12-14, 179, 207]

3 Cascaded connection

In cascaded connection, each manipulation force is independent, and they are connected in series along the flow direction, analogue to "serial circuits" in electronics. Typically, the particles will bed pre-focused or pre-separated by the first force type upstream. Subsequently, the particles follow the fluid flow and enter the downstream. Then, the second manipulation force type further processes the samples in the second separation section. If needed, more separation sections can be connected in sequence. We categorise the cascaded connection system into active-active, active-passive, and passive-passive connections according to the source of each manipulation force, and review the current development of these cascaded connection systems, Figure 2.

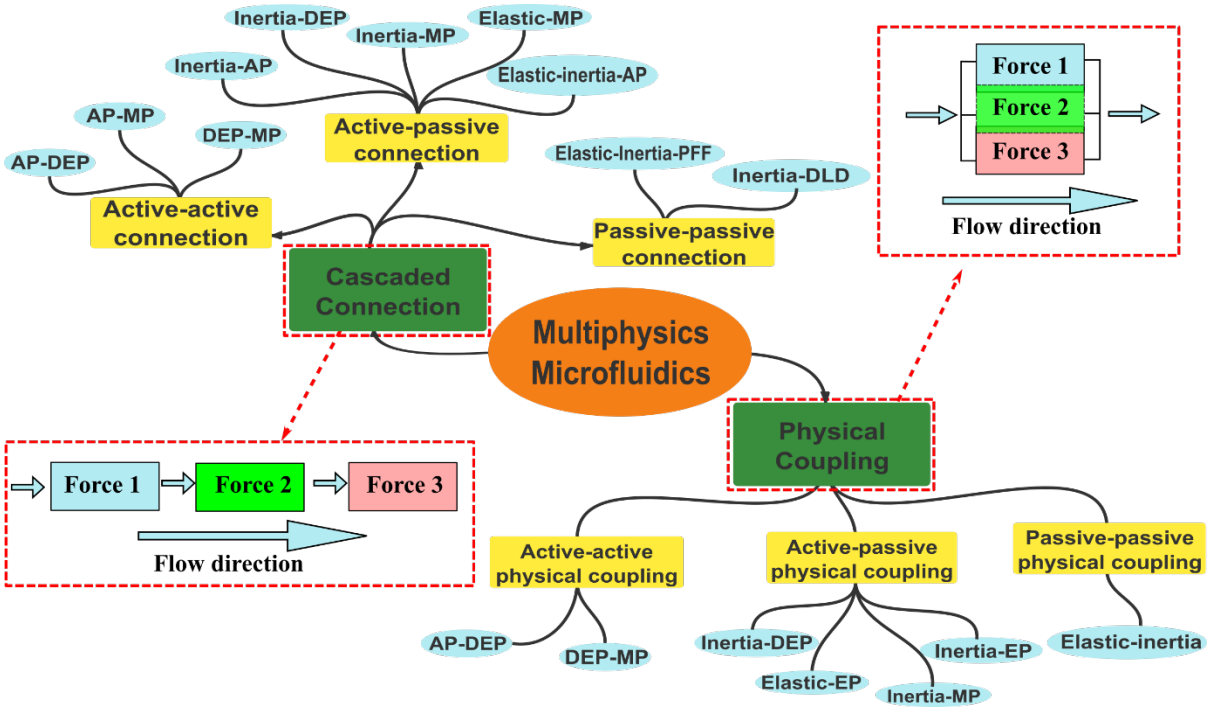

Figure 2. Outline of multiphysics microfluidics. The combination can be in the formats of cascaded connection and physical coupling. Furthermore, we categorise and subdivide them into active-active, active-passive and passive-passive formats based on five main forces: inertial lift, elastic, dielectrophoresis (DEP), magnetophoresis (MP), and acoustophoresis (AP) forces.

3.1 Active-active connection

3.1.1Acoustophoresis-dielectrophoresis (AP-DEP)

Acoustic forces have a broader range of activities within a microchannel and can work spatially, controlling particles/cells in the whole channel.[208] However, the manipulation accuracy of

acoustic force is relatively coarse. In contrast, DEP forces allow for more precise manipulation of single or small particles, but DEP force is only strong enough in the proximity of electrodes.[7] In many ways, sequentially connected acoustic and DEP manipulation play a complementary role in particle focusing,[209] washing, and separation.[210]

Ravula et al. [209] proposed a cascaded system integrating acoustic and DEP manipulation for high-efficiency particle focusing and concentration. The sample mixture was first pre-concentrated and gathered in coarse particle bundles by acoustic forces. In their device, the acoustic force was generated by a bulk lead zirconate titanate (PZT) transducer. In the downstream section, the DEP force generated by an interdigitated DEP electrode further focused the pre-concentrated particles into a single line in a more precise manner. Consecutive connection of AP and DEP units can achieve high-precision focusing performance and minimize problems such as clumping and sticking. Furthermore, the particles can be trapped by switching the DEP force from nDEP to pDEP type.

In biological samples, the suspending buffer medium usually has a high conductivity, which causes adverse Joule heating issues for DEP devices. Therefore, bio-particles need to be transferred to a low-conductivity buffer in DEP systems. Cetin et al. [210] reported a novel system combining acoustic cell washing and DEP cell separation, Figure 3 (A). In their system, acoustic force pushes the particle mixture initially in a high conductivity buffer to the opposite side with low conductivity. Next, the particles were separated based on their dielectric properties by p-DEP and n-DEP. This work used 3D sidewall electrodes to match the high throughput of the acoustic section. The authors employed the mixture of 5-μm latex particles half-coated with aluminium and 5-μm uncoated latex particles to demonstrate cell washing and particle separation.

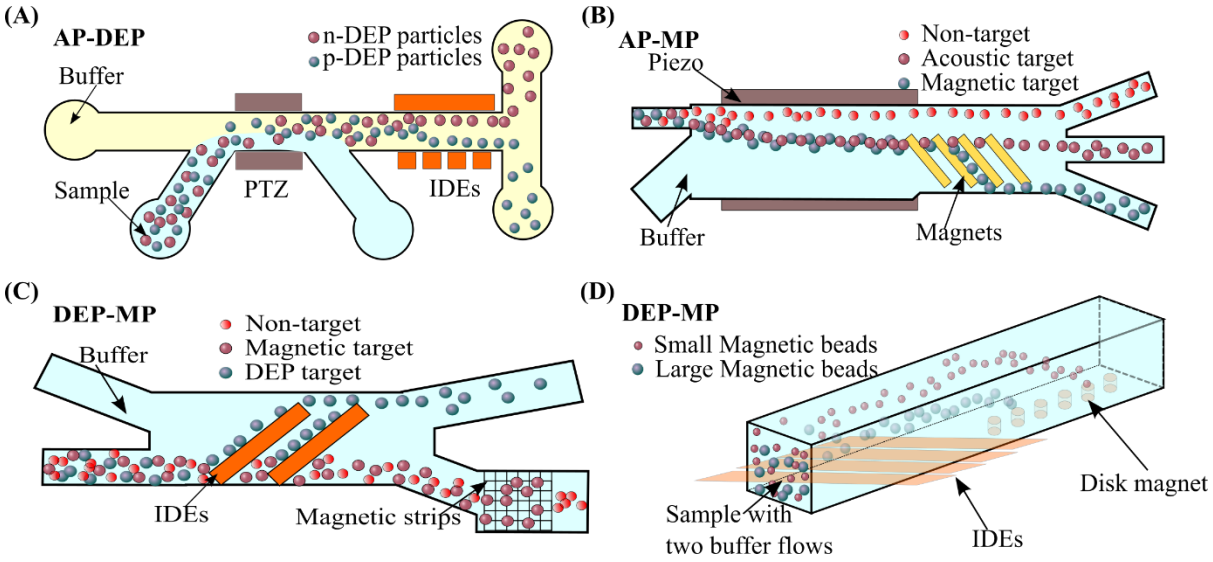

Figure 3. Microfluidic systems with the cascaded combination of active-active connection: (A) The combination of acoustic and DEP forces for particle washing and separation. Acoustic force enables particles to transfer from high conductivity medium to low conductivity medium. Then, particles are separated by pDEP and nDEP forces, generated by 3D sidewall electrodes.[210] (B) An acoustic-magnetic separation (IAMS) device offers multi-parameter sorting of particles based on acoustic and magnetic properties. At the first stage, acoustic radiation force repels the acoustic and magnetic target particles quickly away from the sidewall and filtrate nontarget particles. At the second stage, the magnetic target is deflected further away by the magnetic force and separated from the acoustic targets.[211] (C) A multi-parameter separation device with DEP and magnetic forces. Target cells with DEP tags are first deflected along the angled electrode in the DEP separation unit. Then, microfabricated nickel ferromagnetic strips trap the magnetically labelled targets. And the nontarget cells flow out from the outlet.[212] (D) An integrated multiplex detection system with DEP and magnetophoresis for sorting magnetic beads of different sizes. Magnetic beads with various sizes experience different p-DEP or n-DEP forces and are confined at varied vertical locations in the DEP region. Then, the downstream disk magnet array trapped these magnetic beads at different horizontal locations.[213]

3.1.2 Acoustophoresis-magnetophoresis (AP-MP)

Multi-parameter separation at high purity and throughput is of great importance for many biotechnology applications. Adams et al. [211] developed an integrated acoustic-magnetic separation (IAMS) device, offering multi-parameter sorting of particles based on acoustic and magnetic properties. The sample mixture consisted of acoustic target particles (5-μm green polystyrene particles), magnetic target particles (4.5-μm magnetic microspheres), and

nontargets (1-μm blue polystyrene particles) were examined to demonstrate the functionality of the device. The particle mixture is pinched to one channel sidewall by a co-flowing buffer at the inlet. In the acoustic separation section, the acoustic radiation force moves acoustic and magnetic target particles quickly toward the pressure node near the channel centre. In contrast, nontargets remain in the original path and enter the waste outlet, Figure 3 (B). Subsequently, in the magnetic separation section, magnetic targets are deflected further away by the magnetic force generated by an array of ferromagnetic Ni microstructures. Eventually, magnetic targets are separated from the acoustic target particles. The experimental results demonstrated a high throughput with 10^8 particles per hour and high purities of 94.8% at the magnetic outlet and 89.2% at the acoustic outlet. We should note that the acoustic force has a broad scope of action and may deteriorate the magnetic separation. To eliminate the influence of acoustic forces on magnetic separation, the authors modified the local width of the microchannel to disrupt the acoustic resonance in the magnetic separation section.

3.1.3 Dielectrophoresis-magnetophoresis (DEP-MP)

Although both DEP and MP forces are short-ranged, most effective within the nearfield of electrical and magnetic sources, connecting them in sequence enables sorting multiple biological targets by different tags. Kim and Soh [212] introduced an integrated Dielectrophoretic-Magnetic Activated Cell Sorter (iDMACS) for separating multiple bacterial targets. Two different bacterial clones of *E. coli* MC1061 strain were stained with DEP tags (9.6-μm polystyrene beads) and magnetic tags (50-nm MicroBeads, Miltenyi, Auburn, CA), respectively. The third bacteria clone was used as nontarget cells. The mixture of three bacteria clones flows parallelly with a buffer flow at the inlet, Figure 3(C). In the DEP separation section, the targets with DEP tags experience strong n-DEP, and are selectively deflected along the angled electrodes into the upper outlet. Subsequently, the remnant cells enter the magnetic separation module, where microfabricated nickel ferromagnetic strips trap magnetically labelled targets. Finally, the nontargets elute from the bottom outlet. After a single pass of the iDMACS system at 2.5×10^7 cells/h, the DEP-target cells were enriched 310 times with purity increased from 0.32% to 98.6%. The fraction of magnetic-target cells were concentrated 870 folds, purity raised from 0.11% to 95.6%.

Magnetic microbeads have been widely used as the solid-phase carrier in immunoassays. The efficient manipulation of multiplex magnetic microbeads in microfluidic systems is essential for point-of-care diagnostics. Krishnan et al.[213] designed a microfluidic system to separate superparamagnetic microbeads of different sizes employing DEP and MP types of

magnetic microbeads (1 μm, 2.8 μm, and 5 μm in diameter) were tested, and they showed different DEP properties, Figure 4 (D). At a specific AC signal and frequency, certain magnetic beads experience a p-DEP force and are attracted to the bottom electrode, while others are driven away from the electrode by an n-DEP force. Thus, the magnetic beads are confined at distinct vertical positions. In the magnetic section, an array of NdFeB disk magnets apply vertical magnetic forces on the beads. Depending on their initial vertical sites in the DEP region, the beads are attracted to the magnets at different longitudinal locations. In addition, these beads can be identified by their optical properties. This system could be a good candidate for particle separation, trapping, and multiplex detection.

3.2 Active-passive connection

3.2.1 Inertial lift force- acoustophoretic (Inertia-AP)

Conventional fluorescence-activated cell sorter (FACS) encapsulates cells into the aerosolized droplets, screens cells optically at a single cell level and deflects droplets and cells selectively by an electrostatic field. Microfluidic fluorescent-activated cell sorter (μFACS) is a miniaturized version of the conventional FACS system. μFACS holds many advantages compared to its conventional counterpart. For instance, μFACS eliminates the usage of an aerosol nozzle that may harm cells or bring about safety concerns. In addition, microfluidic devices are disposable to avoid biohazardous clean-up steps. Furthermore, microfluidic devices are much easier for optical alignment. Mutafopulos et al. [214] reported a μFACS device integrating spiral inertial focusing and surface acoustic sorting, Figure 4 (A). Cells are laterally focused into a narrow central region by the counterbalance of inertial lift forces and Dean vortices in a spiral channel. To further confine cells in the vertical direction, two sheath flows are configured vertically at the intersection of the sample flow. Cells are then focused into a tight core stream near the bottom of the channel, which maximizes the effective acoustic force on cells. Subsequently, travelling surface acoustic waves (TSAWs) generated by the tapered interdigital transducer (IDT) deflect the cells when the fluorescent label signal is detected. Three different cell lines were tested, and sorting purities were more than 90% at rates over 3,000 events per second.

Isolation of rare circulating tumour cells (CTCs) from blood samples as liquid biopsy is critical for cancer diagnosis and prognosis. Inertial lift forces have been tailored for label-free separation of CTCs based on the size difference between CTCs and blood cells.[215] However, size-based sorting lacks specificity. On the contrary, label-based cell sorting is more specific. However, labelling multiple sets of surface biomarkers is expensive, labour-intensive, and

time-consuming. Due to the complex nature and heterogeneity of tumours, it is challenging to have high-integrity CTCs separation using a single separation process. To address these issues, Zhou et al. [77] developed a hybrid cell sorting method combining CTCs pre-concentration by a reverse-wavy inertial focusing system and additional single-cell isolation using an acoustophoretic (AP) based μFACS system, Figure 4(B). The fluorescently labelled breast cancer cells were mixed in a 10× diluted whole blood sample. At this first stage, cancer cells are separated from the smaller blood cells in an inertial microfluidic device with a reverse wavy channel, with a 50- to 100-fold enrichment. In the second stage, the pre-enriched sample is further purified by an acoustophoretic μFACS, which delivers another target cell enrichment of 50- and 100- fold. Therefore, the whole process could enrich cells by 2,500- to 10,000-fold, with purity enhanced from ~0.01% to ~40%. We should note that in this work, the pre-concentration by inertial focusing and single cells isolation in AP-μFACS were conducted separately in two individual devices. The pre-concentrated samples were collected and manually transferred into the μFACS system. Therefore, strictly speaking, it is not a "real" seamlessly integrated system. The involvement of manual collection and loading samples introduces the potential risk of rare cell loss, although it avoids the match of flow rate between two processing sections.

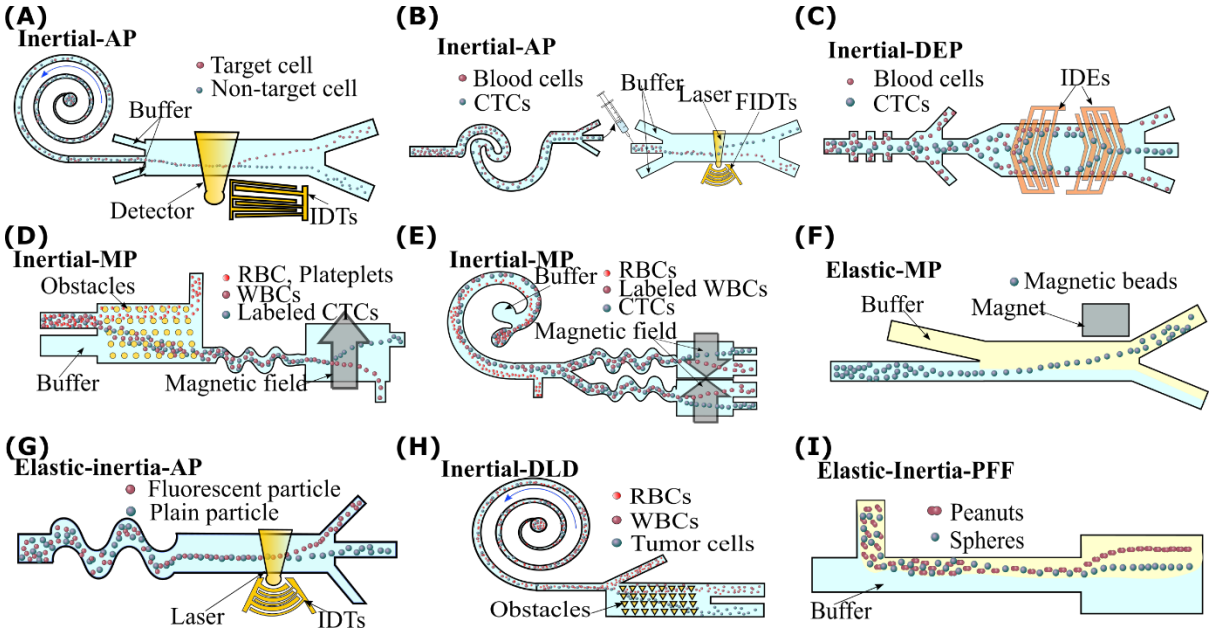

Figure 4. Microfluidic systems with the cascaded combination of active-passive and passive-passive connections: (A) An μFACS system integrated with spiral inertial focusing and acoustic sorting. Sample mixture first focuses into a single line by inertial focusing in a spiral channel and two vertical sheath flows. Then, the fluorescence signal of the labelled cells actuates the IDT, generating an acoustic wave to deflect target cells to the separation outlet.[214]

(B) Combining a label-free inertial focusing device and a label-based AP μFACS system for double-step rare cancer cell separation. Sample mixtures are first pre-enriched 50- to 100- fold in the reverse wavy inertial device. Then, the pre-concentrated samples are further enriched 50- to 100- fold by the AP-μFACS technology. The whole process can highly concentrate cancer cells around 2500- to 10000-fold.[77] (C) An integrated system combines MOFF and DEP technologies for continuous, high-throughput, and precise cancer cell separation. Human cancer cells (MCF-7) with extra-large cells are firstly filtrated out. Cancer cells are further purified at the DEP region.[57] (D) An inertial focusing-enhanced microfluidic CTC isolation platform consists of three microfluidic technologies: deterministic lateral displacement (DLD) pre-sorting, asymmetrical serpentine focusing, and magnetophoresis separation. DLD firstly debulks the blood sample to deplete smaller red blood cells, platelets and unbound magnetic beads. Then, the remaining nucleated cells are focused by inertial forces in the serpentine channel, and cells labelled with magnetic beads are deflected and separated by a magnetic field.[58] (E) A hybrid device consists of spiral inertial sorting, asymmetrical serpentine inertial focusing, and magnetic separation. RBCs and small-size cells are firstly separated in a spiral inertial sorter with high throughput. The remaining mixture of cancer cells and WBCs are aligned in one streamline, and an external magnetic field removes the magnetically labelled WBCs.[216] (F) A two-stage system with an H-shaped microchannel combining viscoelastic focusing and magnetophoretic deflection. The particles are aligned in a single line by the viscoelastic force, and the magnetic beads are deflected into the upper buffer by the attractive magnetic force.[217] (G) The acoustic fluorescence-activated cell sorter (aFACS) consists of elastic-inertial focusing and acoustophoretic sorting. Elastic and inertial lift forces align cells in a single line in a series of repeating curved channels. Then, the focused travelling surface acoustic wave (FTSAW) sorts targets cells based on the fluorescence signal of the cells.[218] (H) A two-stage i-DLD device integrates a spiral inertial sorter and a DLD sorter. In the spiral inertial sorter, massive background cells such as RBCs are removed from the upper outlet. Then, the DLD sorter separates the residual tumor cells and blood cells.[59] (I) An elastic-inertial enhanced PFF (eiPFF) system is comprised of an elastic-inertial straight channel and a sudden expanding segment. PFF in the expanding region amplifies the lateral difference of particles.[219]

3.2.2 Inertial lift force-dielectrophoresis (Inertia-DEP)

Particles migrate to different lateral positions due to the inertial effects in contraction-expansion array channels, termed multi-orifice flow fractionation (MOFF). As one inertial microfluidic technique, MOFF has the advantages of high throughput and simple operation [220].

However, the separation purity is not satisfactory, and a secondary purification module is required. To improve separation performance, Moon et al. [57] proposed one combinatory system for cancer cells separation, taking advantage of MOFF as a massive and fast pre-filtration and DEP as a precise post-processing step, Figure 4 (C). Cancer cells were enriched at the middle outlet in the first region, with a few blood cells accompanied. Subsequently, cells entered an expanded channel with two sets of tangled electrodes. The positive DEP force created by the first set of tangled electrodes attracts all the cells to the sidewall. In the second set of electrodes, only cancer cells experience sufficient DEP force and successfully reach the channel centre. In this device, cancer cell enrichment reached 162-fold at a flow rate of 126 µl/min, and the depletion ratio of red and white blood cells was 99.24% and 94.23%, respectively.

3.2.3 Inertial lift force-magnetophoresis (Inertia-MP)

In addition to DEP, magnetophoresis can be combined with inertial lift force to facilitate the isolation of CTCs. Toner group [58] invented an inertial focusing–enhanced microfluidic CTC separation platform, termed "CTC-iChip". The hybrid system consists of triple working sections: deterministic lateral displacement (DLD), inertial focusing, and magnetophoresis separation, Figure 4 (D). In DLD, the smaller cells below a threshold, such as RBCs, platelets, and unbound magnetics beads, are massively depleted from whole blood by the hydrodynamic force. Then, the remaining nucleated cells move into an asymmetric serpentine channel and align along a single-core stream by inertial forces. Finally, in the third section, target cells labelled with superparamagnetic beads are deflected to the collection channel by the magnetic force, so that labelled and unlabelled cells can be collected separately. This system can isolate CTCs in both positive (tumour antigen-dependent) and negative (tumour antigen-independent) selection modes. In the positive selection mode, CTCs are immunolabelled with magnetic beads based on their expression of tumour-specific antigen (EpCAM). On the contrary, leukocytes are magnetically labelled in the negative selection mode through common leukocyte antigens (CD45 and CD15).[221]

However, DLD and inertial focusing-enhanced magnetophoresis were implemented in two different devices. The DLD device was fabricated on a silicon wafer by silicon deep reactive ion etching. The inertial focusing-enhanced magnetophoresis device was fabricated by the standard polydimethylsiloxane (PDMS) soft lithography. A tubing interconnected two devices, and the output flow rate splitting of the DLD device was externally controlled by a syringe pump. Overall, thedesign led to high fabrication costs and extended setting up time, limiting its application within a clinical setting. To overcome these issues, the group upgraded

the system into a monolithic chip, and all the components were manufactured in a single plastic chip via injection-compression moulding.[163] Furthermore, the on-chip fluidic resistors were used to adjust the waste flow rate of DLD rather than the external syringe pump. These improvements significantly reduced the installation and preparation time, promoting the accessibility of the technology.

Although DLD can debulk blood samples by size-based separation of nucleated cells from smaller red blood cells and platelets, DLD has a clogging issue due to the narrow pillar gap. Moreover, manufacturing precise pillar arrays is costly. Recently, Huang and Xiang [216] reported a similar integrated device by replacing the first stage DLD sorter with a spiral inertial sorter, Figure 4 (E). The first stage gets rid of RBCs from the blood sample by inertial sorting in a spiral channel. Next, the remaining WBCs and CTCs flow into the second serpentine inertial focusing section. Finally, the magnetically labelled WBCs are separated by a strong magnetic field. In this device, the spiral inertial sorter has a much wider channel, eliminating the clogging issue. It should also be highlighted that their integrated device was fabricated by stacking five functional chip layers. In each chip layer, a thin silicon film with designed channel structures was sandwiched by two sheets of polyethylene terephthalate (PET) films. Since all raw materials (such as silicon films and PET films) for the fabrication of the device are at a low cost, the cost for the integrated device can be as low as a few cents.

3.2.4 Elastic lift force-magnetophoresis (Elastic-MP)

Besides the fluid inertia, the viscoelastic properties of the fluid can be utilized for particle manipulation. In practice, many biological fluids,[99, 101] and aqueous solutions of synthetic polymers [103-105] have non-Newtonian properties, such as shear thinning and elasticity.[94] Compared with the inertial lift force, the elastic force not only can focus microscale particles, it can even focus and concentrate submicron to nano-scaled particles.[100, 222] Furthermore, the elastic force can easily align and focus particles at the centreline of a simple straight channel in three dimensions (3D). Therefore, the elastic force can act as an effective pre-focuser for downstream detection and separation.

Del Giudice et al. [217] introduced a hybrid system combining elastic focusing and positive magnetophoresis to separate magnetic particles in an H-shaped microchannel, Figure 4 (F). The magnetic and non-magnetic particles were suspended in a polyacrylamide (PAM, 0.5% w/w) aqueous solution. The viscoelastic force first aligns this particle mixture in a single streamline in a straight rectangular microchannel. Next, a particle-free buffer from a parallel

inlet was introduced to the outlet of the viscoelastic channel at the same flow rate. Finally, a cubic permanent magnet on the side of the channel attracted magnetic beads to the buffer solution and separated them from nontargets. In this device, viscoelastic pre-focusing increases the efficiency of separation. Furthermore, the parallel buffer flow can avoid blocking issues near the magnet wall region. Apart from positive magnetophoresis, integrating elastic focusing with negative magnetophoresis has also been demonstrated.[223, 224] In this case, non-magnetic particles are suspended in a ferrofluid with a viscoelastic base medium. The elastic force-aligned particles are deflected at various speeds and separated by a negative magnetophoretic force.

3.2.5 Elastic lift force- inertial lift force - acoustophoresis (Elastic-Inertia-AP)

Fluorescence-activated cell sorter (FACS) can analyze and sort cells at a single level. In FACS systems, sheath flows are frequently utilized to control the position of particles in the channel for precise detection. However, additional controlled pumps increase the complexity of the operation and sheath flow also dilutes the sample. The three-dimensional focusing capacity of the elastic lift forces can eliminate sheath flows and simplify the overall system. Li et al. [218] developed a novel acoustic FACS (aFACS), in which the elastic and inertial lift forces focus cells in a single file through a series of curved channels. A focused travelling surface acoustic wave (FTSAW) sorts the cells by detecting the fluorescence signal of the passing cells, Figure 4 (G). The breast cancer cells (MCF-7, MDA-231) and human-induced pluripotent stem cell-derived cardiomyocytes (hiPSC-CMs) were tested in the developed aFACS system, and the cell viability was compared with a commercial FACS system Moflo Astrios (Beckman Coulter Life Sciences). The results showed that a high level of cell viability was maintained in the aFACS, only dropping by 3-4%, while the commercial FACS dropped the cell viability by 35-45%.

3.3 Passive-passive connection

3.3.1 Inertial lift force-deterministic lateral displacement (Inertia-DLD)

Besides the active-active and active-passive connections, connecting passive and passive manipulation techniques in series has also been explored.[59] The integration of multiple passive methods is predominant in a resource-low environment since it avoids multiple activating forces. Its operation is simple and has a relatively higher processing throughput.[59] Regarding the passive-passive combination, one strategy is to cascade the same process in sequence, similar to the recirculation of samples through the same processor.[225-228] In this case, the

principles of all the sectors are the same. The other strategy is connecting different passive techniques. The first unit can debulk the raw sample by removing massive background cells in a high-throughput way, significantly shrinking the sample volume. Then, the second sector can further purify the sample with a finer separation resolution.

Xiang et al. [59] devised a two-stage system that combined spiral inertial sorting and DLD, termed i-DLD sorter. In the spiral inertial sorter, massive background blood cells were removed from the blood sample, reducing the blocking issues in the latter DLD sorter, Figure 4 (H). The DLD system separated the residual blood cells at the second stage, further purifying tumour cells. The results showed that 99.95% of background cells were removed. The recovery ratio of the tumour was as high as 91.34%, and the purity was enhanced from 0.001% to 15.48%. Notably, the triangular post DLD sorter is insensitive to flow speed, avoiding matching the operational flow rates between two sorters. Besides, cancer cells and blood cells are focused into the upper half region in the spiral channel, so that the cell-free flow at the bottom half delicately can act as a sheath flow, eliminating the need for an additional sheath flow for DLD.

3.3.2 Elastic lift force-inertial lift force-pinched flow fractionation (Elastic-Inertia-PFF)

Pinched flow fractionation (PFF) is a separation technology that utilizes a laminar flow profile at a suddenly expanded channel.[29] The particles are first pinched against the channel sidewall by a strong sheath flow so that the centres of particles are located at the size-dependent streamlines. Later, the separation distance of particles amplifies in the broadened section because of the hydrodynamic spreading. The combination of differential particle inertial migration and PFF can significantly boost the separation distance. Lu and Xuan [219] demonstrated an enhanced PFF device by adding a long inertial straight channel, Figure 4 (I). The inertial lift forces repel particles away from the nearby channel wall. Since the migration speed is dependent on particle size, particles move at different lateral locations at the end of the straight channel. PFF further magnifies this lateral distance between particles. After that, they replaced the Newtonian base medium with a viscoelastic solution and introduced an additional elastic force into the separation mechanism, termed elasto-inertial pinched flow fractionation (eiPFF).[219] Using eiPFF, they investigated the shape-based separation of spherical and peanut-shaped rigid particles with an equal volume.

4 Physical coupling

As we discussed, the cascaded connection is similar to “serial circuits”, in which fluids and particles continuously pass through each working section, and each manipulating force is

independent. However, the physical coupling format looks like “parallel circuits”, where multiple manipulating forces simultaneously apply to the particles or fluids. The superposition of these forces determines the trajectory and equilibrium locations of cells. A delicate coupling of multiple physics introduce more intriguing phenomena and may enable more precise control of cells and offer various functionalities. This section will describe the physical coupling methods based on the classification of active-active, active-passive, and passive-passive physical couplings.

4.1 Active-active physical coupling

4.1.1 Acoustophoresis-dielectrophoresis (AP-DEP)

A flexible and multi-purpose platform is necessary for the individual handling of cells. As we mentioned above, DEP technology has high spatial accuracy and single-cell manipulation abilities but is only effective on a localized and short-range field near the electrodes.[229] In compensation, acoustic technology benefits long-distance application and 3D manipulation.[230] In addition, according to the equation (7) and (13), the magnitudes of both forces are dependent on the volume of particles (r^3) and the applied voltage. They are also influenced by contrast factors, such as dielectric and acoustic properties. All of them are beneficial for the physical coupling between the acoustic and DEP forces, which can achieve multi-functional and high precise manipulation.

Wiklund et al. [231] coupled dielectrophoresis (DEP) and ultrasonic standing wave (USW) together in a tuneable system to enable simultaneous high-throughput and individual handling of cells. The oblique coupling of the transducer and microchannel transferred the primarily vertical incident acoustic wave into a horizontal one. The DEP force was generated by coplanar electrodes on the bottom surface of the fluidic channel, playing a role in high-precise and single-particle manipulation. A coarse alignment of particles was first performed by the long-distance working region of USW force before entering the electrodes. Then, particles were located based on the force balance between acoustic, DEP, and viscous drag forces. Multi-functions can be achieved by controlling the properties of USW and the electrical field by adjusting the applied frequency or voltage. Dynamic multi-functions, such as particle trapping, particle switching and particle fusion, were demonstrated.

The “virtual” DLD (vDLD) system employs the principle of DLD using virtual acoustic and DEP forces instead of the periodic array of physical pillars.[232] The vDLD system is in real-time control and can avoid the clogging issue of the physical posts of conventional DLD

systems. Because the vDLD takes advantage of acoustic and DEP forces, particles can be sorted based on mechanical properties (compressibility, density) or electrical properties (permittivity). However, in their design, the deterministic displacement of cells was dominated either by acoustic force or DEP force. Two forces cannot work together to define the critical diameter of cells for deterministic sorting. To improve the flexibility and sorting accuracy of the vDLD system, Taybi et al. [196] modified the vDLD system by harnessing both acoustic radiation and DEP forces simultaneously and applied the technique to sort submicrometer particles and extracellular vesicles. Implementing tilted-angle interdigital transducer (IDT) inside the channel can concurrently generate standing surface acoustic waves (TSAW) and a non-uniform electric field, which results in a synergic effect of DEP and acoustic forces on manipulation of particles, Figure 5 (A). The coordination of electrical and acoustic fields in the lateral translation of particles substantially reduces the sorting of the critical diameter of cells (D_{crit}). The results showed that this physical coupling system could significantly reduce the critical diameter down to 100-300 nm and double the lateral migration distance. Furthermore, this system can achieve more than 95% purity and 81% recovery rates of exosome purification. This system has the potentials for multi-criterion sorting based on the different sizes, acoustic contrast factor and polarizability of parties.

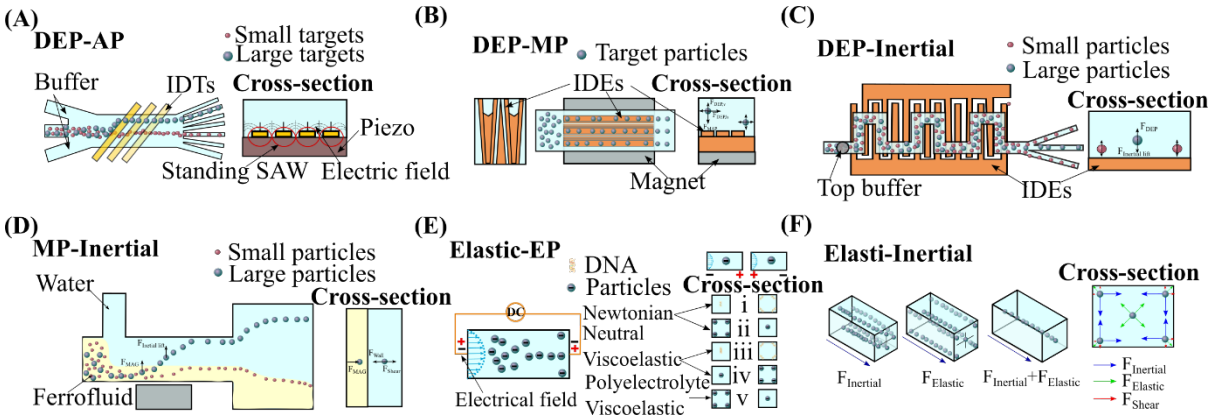

Figure 5. Physical coupling for particle and cell manipulation and separation. (A) A vDLD system sorts submicrometer particles and extracellular vesicles by physical coupling of acoustic and dielectrophoresis forces. The competition of fluid drag force, acoustic radiation force, and DEP force determine the lateral translation of particles, and synthetic effects of electrical and acoustic fields reduce the critical diameter of cells.[196] (B) An interdigitated microelectrode array chip coupled with a permanent magnet underneath. The magnetic force attracts particles to the regions of electrodes and effectively enhances the DEP focusing.[233] (C) A DEP-inertial microfluidic platform for tuneable focusing and separation of particles. An interdigitated electrodes array is embedded under the serpentine inertial microchannel. The

vertical n-DEP force competes with inertial lift forces to adjust the vertical positions of particles. A tiny displacement of particles in the vertical direction can be translated and amplified in the horizontal direction by the secondary flow drag.[56] (D) A hybrid device couples negative magnetophoresis and inertial lift forces for separation and particle washing. The suspended non-magnetic particles in ferrofluid are first compressed into a narrow stream by a sheath flow. Then, significant repulsive magnetic force overcomes inertial lift forces on the large particles to push particles into the buffer water stream.[234] (E) Particle migration phenomenon by a coupling of EP and pressure-driven flow in five distinct categories: (i) polyelectrolyte migration in Newtonian medium, (ii) particle migration in Newtonian medium, (iii) polyelectrolyte migration in neutral viscoelastic medium (PEO), and (iv) particle migration in neutral viscoelastic medium (PEO), (v) particle migration in a polyelectrolyte viscoelastic medium (HA solution).[235] (F) Particle alignment in inertia-dominant flow, elastic-dominant flow and elasto-inertial coupled flow.[107]

4.1.2 Dielectrophoresis-magnetophoresis (DEP-MP)

The combination of DEP and MP can enhance the automotive and programmable functions of microfluidic systems, such as programmable control, simulating electrogenic cells and sensing.[236] Issadore et al. [237] reported a hybrid microfluidic chip by simultaneously coupling DEP and MP forces to trap and move microscopic objects. A 61 × 61 array of pixels of integrated circuit (IC) system can generate strong DEP forces, and a magnetic matrix underneath the DEP pixel array can simultaneously apply MP forces on magnetic particles. In their experiment, a liquid vesicle with iron oxide nanoparticles was first trapped and positioned by DEP force. Then, the magnetic matrix pulled the iron-oxide beads in the vesicle by MP forces so that a thin tether was stretched from the vesicle membrane. In this work, DEP force acts as a body force to hold the micro-object static and MP force as a local force applies precise mechanical stresses on the object. However, two forces are not fully coupled since they are not applied to the same object. Moreover, the micro-object is in a static state.

Simultaneous coupling of DEP and MP forces on the identical particles can be employed to enhance particle focusing efficiency in a continuous flow. In a hybrid system proposed by James et al. [233], a permanent magnet is placed underneath the DEP microelectrode array. The DEP microelectrode array chip composes a series of protrusions structures, which form converging and diverging gaps. Particles undergoing nDEP forces are confined into these gaps along the flow direction (x-axis) by the horizontal component of the DEP force ($F_{DEP,h}$), Figure 5 (B). However, $F_{DEP,h}$ decays rapidly when particles are repelled away from the electrode by

the vertical DEP force ($F_{DEP, v}$), resulting in a weak and chaotic focusing. To pull particles down close to the electrodes, a large permanent magnet underneath the DEP chip attracts particles to a lower position by magnetic force. Therefore, $F_{DEP, h}$ is strong enough to align particles into a single line in the electrode gaps. Coupling of DEP and MP proved a reduced stream width of focused particles and a smaller applicable particle size.

4.2 Active-passive physical coupling

4.2.1 Inertial lift force - dielectrophoresis (Inertia-DEP)

Inertial microfluidics manipulates particles by the fluid inertia-induced lift forces. The technique is superior in simplicity, high throughput and robustness.[35, 63] Nevertheless, the fixed geometry restricts the manipulation capabilities, and lacks flexibility and tunability to adapt to different particle samples.[60] DEP has advantages of precise control, high flexibility for a wide range of particles and tuneable in real-time. However, the flow speed in DEP systems is always limited because a sufficient DEP force needs to be applied to particles for practical application. Coupling DEP forces with inertial lift forces take advantage of both techniques.

Our group [56, 60] explored the physical coupling of inertial lift and DEP forces for tuneable particle focusing and separation in a microfluidic platform, termed DEP-inertial microfluidics. An array of interdigitated electrodes is underneath the serpentine microchannel and generates an n-DEP force. Hence, the vertical DEP force competes with the inertial lift forces delicately along the vertical direction. A tiny displacement of particles in the vertical direction is translated to the horizontal direction and amplified by the secondary flow. In addition, an upper sheath flow at the inlet eliminates the top inertial equilibrium positions so that all the particles can experience sufficient DEP forces near the microelectrodes.[56] Eventually, the separation of various particles can be achieved by adjusting the applied electrical signal, Figure 5 (C). The particle mixtures of 13-μm/5-μm and 13-μm/8-μm were separated respectively by varying the electrical voltage, demonstrating the tuneable separation capability. The DEP-inertial microfluidic system possesses the advantages of high throughput and real-time controllability. It can also bring electrical properties as additional manipulating parameters compared to conventional inertial microfluidics.

4.2.2 Inertial lift force – magnetophoresis (Inertia-MP)

Magnetic solutions with a high concentration of paramagnetic salts or magnetic nanoparticles may harm cells.[157] To avoid the adverse effects on the cells, transferring the particles into another biocompatible buffer is critical. Chen et al. [234] developed a hybrid device for medium

washing and separation of non-magnetic particles through coupling negative magnetophoresis and inertial lift forces. The device consists of coflowing ferrofluid and water streams in a straight microchannel. At the inlet, non-magnetic particles suspended in the ferrofluid are injected from the bottom inlet. A sheath water flow is introduced to the T-junction and pinches the particles mixture into a narrow stream on the sidewall, Figure 5 (D). Next, particles experience a repulsive MP force from the nearby permanent magnet and inertial lift force simultaneously. The MP force competes with inertial lift forces, adjusting the lateral equilibrium positions of particles. By tuning the flow rates of ferrofluid and sheath flows, MP force can overcome the inertial lift forces to migrate large particles across the interface into the buffer water. IN contrast, small particles remain in the ferrofluid because of insufficient magnetic force.

In addition to the coupling of inertial lift and negative MP forces, the combination of inertial lift and positive MP forces for particle separation is also possible. Kumar and Rezai [238] investigated a magneto-hydrodynamic fractionation (MHF) system for continuous and sheathless separation of magnetic particles. Paramagnetic particles first align along the sidewalls of the channel by the active magnetic force from a permanent magnet. The intense competition between magnetic and inertial lift forces would alter the equilibrium position of particles of different sizes. Next, the expansion region increases the distance of particles. Although the inertial force is less dominant than the magnetic force, a more significant displacement can be observed at a high flow rate. Later, the same group modified the device by introducing elastic lift force.[239] The proposed triplex inertia-magneto-elastic (TIME) sorting takes advantage of inertial, magnetic, and elastic forces to focus and separate magnetic particles of various sizes and non-magnetic particles.

4.2.3 Inertial lift force - electrophoresis (Inertia-EP)

In the above discussion, coupling manipulating forces perpendicular to the main flow allows particles to be driven transversely. Electrophoresis, where charged particles are moved by the electrostatic Coulomb force in a uniform electrical field, can enable particles to lead or lag the fluid flow if the electrical field is parallel to the bulk fluid flow. The slip motion of particles interacts with the shear flow, inducing a lateral force - Saffman force to move particles along lateral directions.[240, 241] Particles migrate to the channel centre (low shear region) if they lag behind the main flow. In contrast, particles migrate to the channel walls (high shear region) if they lead the main flow.[242, 243] In a typical inertial microfluidic device, the effect of Saffman force on particles or cells is always ignored since it is too weak. Nevertheless, when coupling

with an external electrical field along the microchannel, the shear-slip effect is enhanced, and the Saffman force is enhanced to alter the inertial focusing positions significantly.

Experimental results of Yuan et al.[244], Li and Xuan,[245] Lochab and Prakash [246] validated the electrophoresis-induced lift force on particles in an inertial flow. The equilibrium positions of particles can be controlled three-dimensionally in the channel. Theoretical studies have been conducted to uncover the fundamental mechanism of electrophoresis-induced lift force. Choudhary et al. [247] studied the effects of electrophoresis on inertial migration and derived an analytical equation for the electrophoresis-induced lift. The team found that the interactions between the electrokinetic slip-driven source dipole field and the stresslet field due to the particle resistance to strain in Poiseuille flow cause electrophoresis-induced lift force. Khair and Kabarowski [243] calculated the cross-stream electrophoresis-induced lift force in a weak inertial flow. The magnitude of the lift force was derived based on the simplification of unbounded, steady and simple shear flow. The results suggested that the cumulative effects of weak fluid inertia are responsible for or at least contributes significantly to the induced lift force. Furthermore, Prohm and co-workers [248-250] theoretically investigated the feedback control of particle inertial equilibrium positions using constant and time-varying axial forces.

4.2.4 Elastic lift force - electrophoresis (Elastic-EP)

Besides the physical coupling of electrophoresis and Newtonian fluid flow, several works explored the coupling of electrophoresis and non-Newtonian viscoelastic fluids.[222, 235, 245] Ranchon et al. [222] designed a funnel-shaped device by combining hydrodynamic and EP to simultaneously enrich and separate DNA in a viscoelastic polyvinylpyrrolidone (PVP) solution. The team applied a counter electric field against the flow direction to hinder the motion of a charged solution. The tuneable electric field resulted in a shear disturbance near the DNA. The induced elastic force pushed the DNA to the wall area. Furthermore, at the funnel section of the chip, the team observed that the DNA would be attracted back forming an enrichment area if the EP force exceeds the hydrodynamic force. The stagnation point would be different due to the various molecular weights (MW), resulting in DNA separation and enrichment simultaneously.

Li and Xuan [245] investigated the EP effect on charged polystyrene particles in viscoelastic polyethylene oxide (PEO) solution. An opposite phenomenon was observed com[ared to that in a Newtonian fluid. Particles move to the centerline of the channel if they lead the flow by positive EP force. Conversely, particles lagging behind the flow migrate to the sidewall. The

team highlighted that the extra induced lift force is generated because of the synergy between electrophoretic particle motion and local flow. Furthermore, with the increase in the strength of the electric field, significant migration can be observed because of the enhanced EP lift fore.

Akash et al. [251] discovered an opposite migration phenomenon of EP effect in PEO solution. When electrophoresis is in the opposite direction of the main flow, the polystyrene spheres migrate to the centerline instead of the wall region. Reversing the electrophoresis pushes the particles toward the channel walls. These phenomena are similar to that in a Newtonian fluid and opposite to that in a viscoelastic fluid [245]. This discrepancy is attributed to the fact that the PEO concentration is too low (250 ppm) in this work, far less than the overlap concentration c* (473 ppm for PEO, Mw =5 MDa), so that polymer coils in the solution have no effective entanglement [65].

To obtain a holistic view of the EP effect, Serhatlioglu et al. [235] systematically studied and summarized the EP effects in Newtonian and viscoelastic fluids, Figure 5 (E). They classified the EP on particle migration into four different categories (i) polyelectrolyte migration in Newtonian medium, (ii) particle migration in Newtonian medium, (iii) polyelectrolyte migration in neutral viscoelastic medium (PEO), and (iv) particle migration in neutral viscoelastic medium (PEO). Furthermore, the team introduced a fifth category, particle migration in a polyelectrolyte viscoelastic medium (HA solution). In HA solution, the charged polystyrene (PS) particles migrate to the channel centre when EP is countercurrent with the channel flow, and to the wall area if EP is in the concurrent direction. Although PEO and HA express similar viscoelastic properties, an opposite trend of particle migration under EP was observed between HA and PEO solutions. Based on the polyelectrolyte nature of HA, the team proposed an electrode-viscoelastic migration (EVM) theory to explain the counterintuitive phenomenon.

4.3 Passive-passive physical coupling

4.3.1 Elastic-inertial lift force (Elastic-inertia)

In an elasticity-dominated flow (Re≈0, Wi>0), particles migrate towards the centerline and four corners of a rectangular channel, which corresponds to the low first normal stress regions, Figure 5 (F).[107] However, these multiple locations cannot be directly applied to particle separation and three-dimensional focusing. Therefore, fluid inertia is introduced to couple with elastic force and remove the four-cornered equilibrium positions. The inertial lift force (wall-lift force) can disturb particle positions at channel corners, repelling particles to the centerline.

Therefore, coupling elastic force and inertial lift force can achieve a single focusing position at the centerline.[38]

Elasto-inertial focusing has been conducted in various viscoelastic solutions such as PEO,[252, 253] HA [254] and DNA.[99] For example, Lim et al. [254] investigated the elasto-inertial focusing in hyaluronic acid (HA) solution. The interaction between fluid inertial and elastic rheology enhanced the particle focusing in the weak elastic fluid (El~0.1). The flow rate of elasto-inertial focusing is three to four orders of magnitude higher than that of the conventional viscoelastic focusing. The focusing performance can improve with increasing flow rate. The particles can align to the centerline under a broad range of Reynolds numbers ($10\sim10^4$). They also demonstrated deterministic focusing of rigid spherical beads, deformable WBCs, and polyethylene glycol (PEG) particles.

Furthermore, coupling elastic and inertial forces has been tailored for particle and cell separations in straight,[96] curved [255] and expansion-contraction array channels [256, 257] etc. For example, Zhou et al.[255] explored controllable particle separation by tuning elasto-inertial effects in a wavy inertial channel. The elasto-inertial interaction is tunable by adjusting flow rates and the polymer concentration of viscoelastic fluids. The new-balanced force competition between inertial, secondary drag and elastic forces can modify the equilibrium positions in the curved channel. The results divided three separation thresholds among 0.3-10 μm particles. The device can simultaneously separate three particles of different sizes into each subpopulation.

5 Discussion and perspectives

This paper first discussed and compared the mechanism of five main manipulating forces in microfluidics: inertial lift, elastic, DEP, magnetic and acoustic forces. Next, we classified multiple physics combinations into two types and reviewed the latest development of systems reported in the literature. The motivation of multiple physics combinations is based on the demands for manipulation and separation of complex samples that devices based on a single physics are intrinsically insufficient to fulfil the tasks. For example, when a particle sample has more than two subpopulations or a binary mixture with overlapping properties, a single technology based on one selection criterion is not good enough for a complete fractionation. Therefore, combining other technologies based on different physics can offer additional separation criteria for further purification. Besides, every technique has its advantages and disadvantages. A careful combination of various techniques may reduce their limitations while

keeping the advantages. One scheme for high throughput processing and single-cell precise manipulation is to combine both long-range and short-range manipulation forces in a single device. The long-range forces, such as acoustic and hydrodynamic forces (inertial and elastic forces), can act as a coarse manipulation to confine a large population of cells within a restricted space. Then, the succeeding short-range forces within the region, such as DEP and magnetic forces, can more delicately control individual cells. Therefore, the integrated system can take both advantages of high throughput and precise single-cell level manipulation.

The combination of multiple physics includes cascaded connection and physical coupling. In the former, the manipulating forces induced from each physics are independent, neither interfering with each other nor acting on the particles/cells simultaneously. The only connection between them is the fluid flow between upstream and downstream. In contrast, in the physical coupling, several physics apply to the identical particles or interact to tune the magnitude and direction of the resultant manipulating forces. In most reports, the combination is limited to two physics for both cascaded connection and physical coupling. Three physics or more are rarely combined,[58] manily because of the complexity of device design and coupling mechanism.

For cascaded connection, although two physics do not interfere each other directly, they are linked by the fluid flow. The upstream fluid will enter the downstream, so the upstream and downstream flow rates must match. However, as we know, some techniques are functional at a high flow speed, such as inertial microfluidics, while others are only suitable for a low flow speed, such as DEP. The difficulty brought by this is how to tune the flow speed up and down at different functional units while ensuring the matching of the fluid flow rate. One feasible solution is to adjust the channel cross-sectional area at each section to control the linear flow speed.[57, 223, 224] The other solution is to deplete or add partial fluids to reduce/increase the flow downstream, so that flow speed can be optimised to suit the second physics.[57, 58, 216] For this purpose, it is necessary to carefully adjust the fluid resistance of each outlet at the fluid division section. It is worth noting that the downstream second manipulating section (based on the second physics) becomes the resistance of one branch at the first unit, making it difficult to calculate the flow resistance, especially in a complicated channel structure. This does bring challenges to the design of devices to combine two physics in series. Fortunately, the flow in microfluidics is laminar. Computational fluid dynamics can reasonably simulate the fluid flow distribution in each branch and guide the design of bifurcating channels. The third solution is

to add a micro-pump between the connective units to adjust the flow speed for the second one, which inevitably complicates the operation of the overall system.

Regarding the design of the functionality of each unit, in general, there are three combinations in the cascaded connection: (i) focusing + sorting; (ii) filtration + filtration/separation; (iii) separation + separation. In the first case, the first force is to confine the sample in a limited space, such as along a single moving trajectory, and the second force will sort cells into different populations,[214, 218, 223, 224] Figure 6 (A). In the second case, the first force filtrates a large population of background cells from the targets, and the debulked sample can then be further purified by the second force unit,[57, 58, 77, 216] Figure 6 (B). Under this condition, both two manipulating forces are effective only on the background cells. This is especially advantageous for the situation where target cells are rare in the mixture. In the third case, where samples contain many subpopulations, each force specifically sorts out one subpopulation from the sample in one unit,[58, 211, 212] Figure 6 (C). This combination can get a purified sample of each population.

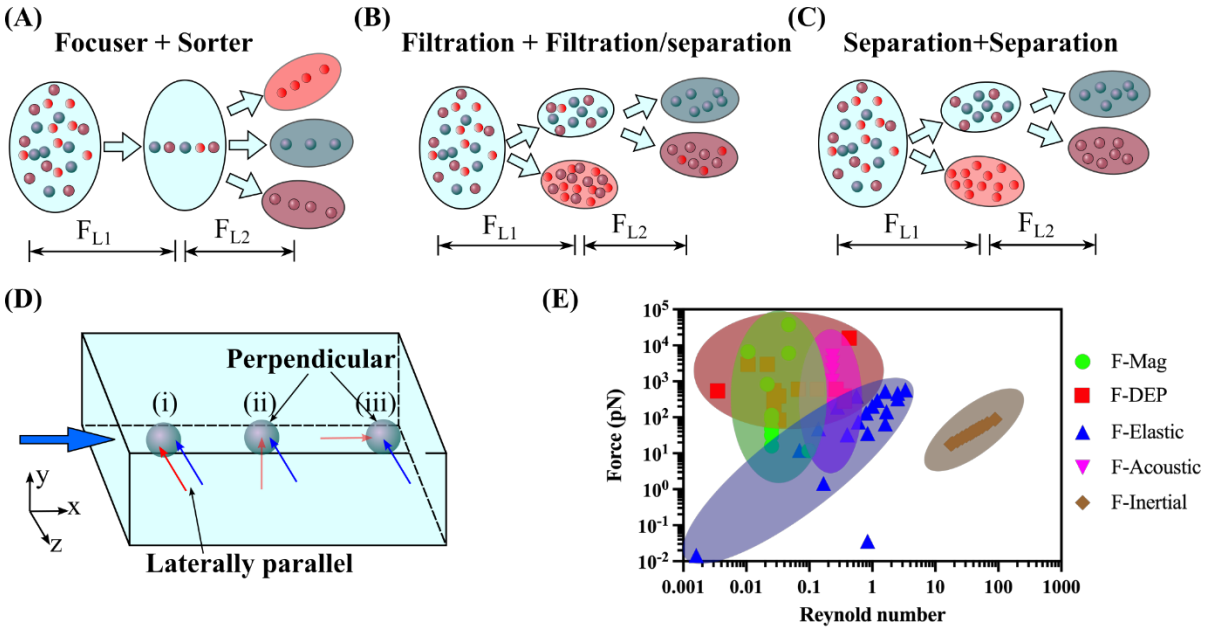

Figure 6. (A-C) Cascaded connection of two functional forces for particle separation. (A) Lateral force 1 (F_{L1}) focus and align all the particles along a single path, and lateral force 2 (F_{L2}) deterministically sort particles into different outlets. (B) F_{L1} and F_{L2} are to filtrate the background cells (red and brown dots) and enrich target particles (blue dots) in series. This applies to the situation where target cells are rare in the mixture. (C) F_{L1} separates red particles in section 1, and F_{L2} sorts up blue and brown particles downstream. Therefore, three particles can be separated respectively. This is especially useful for the fractionation of samples with

multiple components. (D) Two forces are acting on the target particles and coupling at different directions: (i) parallelly along the lateral direction, and perpendicularly with (ii) one in the vertical direction and the other along the lateral direction, (iii) one in main flow direction and the other along the lateral direction. (E) The comparison of different manipulating forces in microfluidics, including inertial lift, elastic, DEP, magnetic and acoustic forces. The force magnitudes are calculated based on the reported literature.[63, 64, 96, 97, 125, 126, 154, 233, 258-265] The particle diameter is 10 μm.

For physical coupling, two or more manipulating forces are simultaneously applying to the cells. The manipulating forces can be parallel or perpendicular. The cells can migrate at a faster differential speed when the directions of two forces are the same, or counteracted and balanced at different lateral positions if the two forces are in opposite directions,[38, 196, 234] Figure 6 (D). In addition, the manipulating forces can be coupled perpendicularly. For example, if the lateral manipulating force is not uniform along the vertical direction, the second manipulating force along the vertical direction can levitate particles to different vertical locations. In this way, the second vertical force can control the magnitude and direction of the first lateral force on particles.[56, 60, 233] Furthermore, the manipulating force can also be in the flow direction, so that particles will lead or lag the flow if the applied force is in the same or an opposite direction of the main flow. A lateral force due to the shear-slip motion of particles – Saffman force can be induced.[240, 241] The Saffman force contributes to or competes with the lateral manipulating force (such as inertial lift force and elastic force) to promote or resist the lateral migration of particles, consequently modifying the final lateral equilibrium positions.[235, 245]

Physical coupling provides several superior advantages. The first is to extend the applicable manipulation range of particle size down to a smaller scale. Since all manipulating forces are proportional to the higher orders of particle size than fluid drag force, such as $F_{DEP} \sim r^3$, $F_{MP} \sim r^3$, $F_{AP} \sim r^3$, $F_{EL} \sim r^3$, $F_{Inertial} \sim r^4$, $F_{Drag} \sim r$. We can see that the manipulating forces drop faster than the drag force with decreasing particle size. The forces will become too weak to overcome the drag force for effective particle manipulation when the particle is too small. Therefore, coupling multiple forces can strengthen the overall manipulating force, and the effective manipulation of submicron and even nanoparticles becomes possible.[196,222] The second benefit is to offer more flexible and precise control of particles in three dimensions. A single manipulating force can only confine particles at finite locations, and the characteristic distribution of forces limits the equilibrium positions. For example, inertial lift force in a square channel can focus particles at four equilibrium positions within the channel cross-section.

Viscoelastic force focuses particles at the four corners and the channel centerline. Coupling with an additional force such as DEP or EP forces, the location and the number of the final equilibrium positions can be modified and tuned precisely in real-time. The third advantage is to offer more controlling parameters and selection parameters for cell manipulation and separation. For example, physical coupling of acoustic and DEP forces can distinguish cells based on size, compressibility and dielectric properties, which brings up more flexibility and capability in cell isolation.

To couple multiple physics effectively, the magnitude of the coupled forces should be in the same order of magnitude, so that neither of them will be dominant and they can compete with each other. We calculated the typical magnitudes of five manipulating forces from the reported literature and summarized them in Figure 6 (E). Figure 6 (E) shows overlapped regions between these five manipulating forces. These regions indicate a vast potential to combine them in one device. To date, there is no report regarding the coupling of acoustic and magnetic forces, and coupling them may provide a versatile platform to manipulate cells based on both deformability and magnetic properties. Moreover, coupling acoustic and viscoelastic forces may discover intriguing new phenomena and open up a brand new field where the non-Newtonian viscoelastic properties, acoustic radiation force and acoustic streaming can work cooperatively. The secondary flows induced by the second normal stress difference in viscoelastic fluids may promote the fluid mixing performance of the acoustic streaming.

To conclude, multiphysics microfluidics is still in its infant stage, although some pioneering studies have been conducted. Most of the reported literature is regarding cascaded connection, and fewer works are exploring the physical coupling. Multiphysics microfluidics has obvious advantages and benefits compared to traditional single-physics microfluidics. There is a broad region to be explored, and a vast possibility is to be fulfilled. By combining multiple physics, flexible, delicate, versatile, and even intelligent platforms can be developed for particle and cell manipulation and separation.

Author contributions

Nam-Trung Nguyen: Proposed the idea and designed the project. **Jun Zhang**: Proposed the idea and designed the project, contributed to the final manuscript. **Haotian Cha**: Developed the theory, interpreted the collected data, drew the figures and took the lead in writing the manuscript. **Hedieh Fallahi**: Collected and interpreted data and illustrated the Inertial force part. **Yuchen Dai**: Contributed to the revision of the manuscript and modification of the figures.

Dan Yuan: Collected and interpreted data and illustrated the Elastic force part. **Hongjie An**: Contributed to the revision of the manuscript and identified the technical terms of the paper. All authors provided critical feedback and helped shape the research, analysis, and manuscript.

Acknowledgements

Authors acknowledge the support from the Australian Research Council (ARC) Discovery Project (Grant No. DP180100055), ARC DECRA fellowship (Grant No. DE210100692), ARC Future Fellowships (FT180100361) and Alfred Deakin Postdoctoral Research Fellowship.

Conflict of interest statement

The authors have declared no conflict of interest.

ReferencesUncategorized References

1 E. K. Sackmann, A. L. Fulton and D. J. Beebe, *Nature*, 2014, **507**, 181-189.
2 C. Jin, S. M. McFaul, S. P. Duffy, X. Deng, P. Tavassoli, P. C. Black and H. Ma, *Lab Chip*, 2014, **14**, 32-44.
3 H. Kimura, Y. Sakai and T. Fujii, *Drug metabolism and pharmacokinetics*, 2018, **33**, 43-48.
4 M. Karimi, S. Bahrami, H. Mirshekari, S. M. M. Basri, A. B. Nik, A. R. Aref, M. Akbari and M. R. Hamblin, *Lab on a Chip*, 2016, **16**, 2551-2571.
5 G. M. Whitesides, *nature*, 2006, **442**, 368-373.
6 J. Y. Chan, A. B. Ahmad Kayani, M. A. Md Ali, C. K. Kok, B. Y. Majlis, S. L. L. Hoe, M. Marzuki, A. S.-B. Khoo, K. Ostrikov and M. A. Rahman, *Biomicrofluidics*, 2018, **12**, 011503.
7 B. Çetin and D. Li, *Electrophoresis*, 2011, **32**, 2410-2427.
8 H. Zhang, H. Chang and P. Neuzil, *Micromachines*, 2019, **10**, 423.
9 J. Zhu, T. R. J. Tzeng and X. Xuan, *Electrophoresis*, 2010, **31**, 1382-1388.
10 F. Alnaimat, S. Dagher, B. Mathew, A. Hilal-Alnqbi and S. Khashan, *The Chemical Record*, 2018, **18**, 1596-1612.
11 Y. Zhang and N.-T. Nguyen, *Lab on a Chip*, 2017, **17**, 994-1008.
12 P. Zhang, H. Bachman, A. Ozcelik and T. J. Huang, *Annual Review of Analytical Chemistry*, 2020, **13**, 17-43.
13 X. Ding, P. Li, S.-C. S. Lin, Z. S. Stratton, N. Nama, F. Guo, D. Slotcavage, X. Mao, J. Shi and F. Costanzo, *Lab Chip*, 2013, **13**, 3626-3649.
14 Y. Q. Fu, J. Luo, N.-T. Nguyen, A. Walton, A. J. Flewitt, X.-T. Zu, Y. Li, G. McHale, A. Matthews and E. Iborra, *Progress in Materials Science*, 2017, **89**, 31-91.
15 T. Yang, Y. Chen and P. Minzioni, *Journal of Micromechanics and Microengineering*, 2017, **27**, 123001.
16 A. Atajanov, A. Zhbanov and S. Yang, *Micro and Nano Systems Letters*, 2018, **6**, 1-16.
17 Q. Zhao, H.-W. Wang, P.-P. Yu, S.-H. Zhang, J.-H. Zhou, Y.-M. Li and L. Gong, *Frontiers in bioengineering and biotechnology*, 2020, **8**, 422.
18 H. Zhang and K.-K. Liu, *Journal of the Royal Society interface*, 2008, **5**, 671-690.
19 D. Gao, W. Ding, M. Nieto-Vesperinas, X. Ding, M. Rahman, T. Zhang, C. Lim and C.-W. Qiu, *Light: Science & Applications*, 2017, **6**, e17039-e17039.
20 L. Lin, X. Peng, X. Wei, Z. Mao, C. Xie and Y. Zheng, *ACS nano*, 2017, **11**, 3147-3154.
21 R. Piazza, *Soft Matter*, 2008, **4**, 1740-1744.
22 Y. Qian, S. L. Neale and J. H. Marsh, *Scientific reports*, 2020, **10**, 1-11.
23 E. H. Hill, J. Li, L. Lin, Y. Liu and Y. Zheng, *Langmuir*, 2018, **34**, 13252-13262.
24 F. Tian, Z. Han, J. Deng, C. Liu and J. Sun, *View*, 2021, 20200148.
25 X. Fan, C. Jia, J. Yang, G. Li, H. Mao, Q. Jin and J. Zhao, *Biosensors and Bioelectronics*, 2015, **71**, 380-386.
26 X. Chen and J. Shen, *Journal of Chemical Technology & Biotechnology*, 2017, **92**, 271-282.
27 N. Xiang, Q. Li and Z. Ni, *Anal. Chem.*, 2020, **92**, 6770-6776.
28 X. Lu and X. Xuan, *Anal. Chem.*, 2015, **87**, 6389-6396.
29 M. Yamada, M. Nakashima and M. Seki, *Anal. Chem.*, 2004, **76**, 5465-5471.
30 S. Wang, Z. Liu, S. Wu, H. Sun, W. Zeng, J. Wei, Z. Fan, Z. Sui, L. Liu and X. Pan, *Electrophoresis*, 2021, 1-7.
31 J. McGrath, M. Jimenez and H. Bridle, *Lab on a Chip*, 2014, **14**, 4139-4158.

32 A. Hochstetter, R. Vernekar, R. H. Austin, H. Becker, J. P. Beech, D. A. Fedosov, G. Gompper, S.-C. Kim, J. T. Smith and G. Stolovitzky, *ACS nano*, 2020, **14**, 10784-10795.
33 T. Salafi, Y. Zhang and Y. Zhang, *Nano-Micro Letters*, 2019, **11**, 1-33.
34 Q. Zhao, D. Yuan, J. Zhang and W. Li, *Micromachines*, 2020, **11**, 461.
35 J. Zhang, S. Yan, D. Yuan, G. Alici, N.-T. Nguyen, M. E. Warkiani and W. Li, *Lab on a Chip*, 2016, **16**, 10-34.
36 Y. Gou, Y. Jia, P. Wang and C. Sun, *Sensors*, 2018, **18**, 1762.
37 J. Zhou and I. Papautsky, *Microsystems & Nanoengineering*, 2020, **6**, 1-24.
38 D. Yuan, Q. Zhao, S. Yan, S.-Y. Tang, G. Alici, J. Zhang and W. Li, *Lab Chip*, 2018, **18**, 551-567.
39 F. Tian, L. Cai, J. Chang, S. Li, C. Liu, T. Li and J. Sun, *Lab Chip*, 2018, **18**, 3436-3445.
40 J. Zhang, D. Yuan, R. Sluyter, S. Yan, Q. Zhao, H. Xia, S. H. Tan, N.-T. Nguyen and W. Li, *IEEE Trans. Biomed. Circuits Syst.*, 2017, **11**, 1422-1430.
41 C. W. Shields IV, C. D. Reyes and G. P. López, *Lab on a Chip*, 2015, **15**, 1230-1249.
42 M. E. Warkiani, B. L. Khoo, L. Wu, A. K. P. Tay, A. A. S. Bhagat, J. Han and C. T. Lim, *Nature protocols*, 2016, **11**, 134-148.
43 P. Bankó, S. Y. Lee, V. Nagygyörgy, M. Zrínyi, C. H. Chae, D. H. Cho and A. Telekes, *Journal of hematology & oncology*, 2019, **12**, 1-20.
44 C. S. Luke, J. Selimkhanov, L. Baumgart, S. E. Cohen, S. S. Golden, N. A. Cookson and J. Hasty, *ACS synthetic biology*, 2016, **5**, 8-14.
45 A. Schaap, J. Dumon and J. Den Toonder, *Microfluidics and Nanofluidics*, 2016, **20**, 1-11.
46 M. A. Faridi, H. Ramachandraiah, I. Banerjee, S. Ardabili, S. Zelenin and A. Russom, *Journal of nanobiotechnology*, 2017, **15**, 1-9.
47 J. Cama, M. Voliotis, J. Metz, A. Smith, J. Iannucci, U. F. Keyser, K. Tsaneva-Atanasova and S. Pagliara, *Lab on a Chip*, 2020, **20**, 2765-2775.
48 S. Patel, D. Showers, P. Vedantam, T.-R. Tzeng, S. Qian and X. Xuan, *Biomicrofluid*, 2012, **6**, 034102.
49 T. Salafi, K. K. Zeming and Y. Zhang, *Lab on a Chip*, 2017, **17**, 11-33.
50 K. Choi, H. Ryu, K. J. Siddle, A. Piantadosi, L. Freimark, D. J. Park, P. Sabeti and J. Han, *Analytical chemistry*, 2018, **90**, 4657-4662.
51 S. Gholizadeh, M. S. Draz, M. Zarghooni, A. Sanati-Nezhad, S. Ghavami, H. Shafiee and M. Akbari, *Biosensors and Bioelectronics*, 2017, **91**, 588-605.
52 T.-W. Lo, Z. Zhu, E. Purcell, D. Watza, J. Wang, Y.-T. Kang, S. Jolly, D. Nagrath and S. Nagrath, *Lab on a Chip*, 2020, **20**, 1762-1770.
53 Y. Belotti and C. T. Lim, *Analytical Chemistry*, 2021, **93**, 4727-4738.
54 S. Yan, J. Zhang, D. Yuan and W. Li, *Electrophoresis*, 2017, **38**, 238-249.
55 Y. Wang, J. Wang, J. Cheng, Y. Zhang, G. Ding, X. Wang, M. Chen, Y. Kang and X. Pan, *IEEE Sensors Journal*, 2020, **20**, 14607-14616.
56 J. Zhang, D. Yuan, Q. Zhao, S. Yan, S.-Y. Tang, S. H. Tan, J. Guo, H. Xia, N.-T. Nguyen and W. Li, *Sensors and Actuators B: Chemical*, 2018, **267**, 14-25.
57 H.-S. Moon, K. Kwon, S.-I. Kim, H. Han, J. Sohn, S. Lee and H.-I. Jung, *Lab Chip*, 2011, **11**, 1118-1125.
58 E. Ozkumur, A. M. Shah, J. C. Ciciliano, B. L. Emmink, D. T. Miyamoto, E. Brachtel, M. Yu, P.-i. Chen, B. Morgan and J. Trautwein, *Sci. Transl. Med.*, 2013, **5**, 179ra147.
59 N. Xiang, J. Wang, Q. Li, Y. Han, D. Huang and Z. Ni, *Anal. Chem.*, 2019, **91**, 10328-10334.

60 J. Zhang, S. Yan, G. Alici, N.-T. Nguyen, D. Di Carlo and W. Li, *RSC Adv.*, 2014, **4**, 62076-62085.
61 M. Tayebi, D. Yang, D. J. Collins and Y. Ai, *Nano Lett.*, 2021, **21**, 6835-6842.
62 W. Tang, S. Zhu, D. Jiang, L. Zhu, J. Yang and N. Xiang, *Lab on a Chip*, 2020, **20**, 3485-3502.
63 D. Di Carlo, *Lab Chip*, 2009, **9**, 3038-3046.
64 D. Huber, A. Oskooei, X. Casadevall i Solvas, A. Demello and G. V. Kaigala, *Chemical reviews*, 2018, **118**, 2042-2079.
65 R. Nasiri, A. Shamloo, S. Ahadian, L. Amirifar, J. Akbari, M. J. Goudie, K. Lee, N. Ashammakhi, M. R. Dokmeci and D. Di Carlo, *Small*, 2020, **16**, 2000171.
66 A. E. Reece and J. Oakey, *Physics of Fluids*, 2016, **28**, 043303.
67 J. Zhou, A. Kulasinghe, A. Bogseth, K. O'Byrne, C. Punyadeera and I. Papautsky, *Microsystems & nanoengineering*, 2019, **5**, 1-12.
68 S. Shen, C. Tian, T. Li, J. Xu, S.-W. Chen, Q. Tu, M.-S. Yuan, W. Liu and J. Wang, *Lab Chip*, 2017, **17**, 3578-3591.
69 X. Bian, Y. Lan, B. Wang, Y. S. Zhang, B. Liu, P. Yang, W. Zhang and L. Qiao, *Analytical chemistry*, 2016, **88**, 11504-11512.
70 S. Ghadami, R. Kowsari-Esfahan, M. S. Saidi and K. Firoozbakhsh, *Microfluidics and Nanofluidics*, 2017, **21**, 1-10.
71 U. Sonmez, S. Jaber and L. Trabzon, *Journal of Micromechanics and Microengineering*, 2017, **27**, 065003.
72 X. Lu, J. J. M. Chow, S. H. Koo, T. Y. Tan, B. Jiang and Y. Ai, *Analytical Chemistry*, 2020, **92**, 15579-15586.
73 Y. Zhou, Z. Ma and Y. Ai, *Microsystems & nanoengineering*, 2018, **4**, 1-14.
74 M. Li, H. E. Muñoz, A. Schmidt, B. Guo, C. Lei, K. Goda and D. Di Carlo, *Lab on a Chip*, 2016, **16**, 4458-4465.
75 M. E. Warkiani, A. K. P. Tay, B. L. Khoo, X. Xiaofeng, J. Han and C. T. Lim, *Lab on a Chip*, 2015, **15**, 1101-1109.
76 D. Jiang, D. Huang, G. Zhao, W. Tang and N. Xiang, *Microfluidics and Nanofluidics*, 2019, **23**, 1-11.
77 Y. Zhou, Z. Ma and Y. Ai, *RSC advances*, 2019, **9**, 31186-31195.
78 H. W. Hou, M. E. Warkiani, B. L. Khoo, Z. R. Li, R. A. Soo, D. S.-W. Tan, W.-T. Lim, J. Han, A. A. S. Bhagat and C. T. Lim, *Scientific reports*, 2013, **3**, 1-8.
79 K. J. Smith, J. A. Jana, A. Kaehr, E. Purcell, T. Opdycke, C. Paoletti, L. Cooling, D. H. Thamm, D. F. Hayes and S. Nagrath, *Lab Chip*, 2021, **21**, 3559-3572.
80 S. Zhu, F. Jiang, Y. Han, N. Xiang and Z. Ni, *Analyst*, 2020, **145**, 7103-7124.
81 H. Fallahi, S. Yadav, H.-P. Phan, H. Ta, J. Zhang and N.-T. Nguyen, *Lab on a Chip*, 2021, **21**, 2008-2018.
82 H. Jeon, B. Jundi, K. Choi, H. Ryu, B. D. Levy, G. Lim and J. Han, *Lab on a Chip*, 2020, **20**, 3612-3624.
83 A. A. S. Bhagat, H. W. Hou, L. D. Li, C. T. Lim and J. Han, *Lab Chip*, 2011, **11**, 1870-1878.
84 J. S. Dudani, D. E. Go, D. R. Gossett, A. P. Tan and D. Di Carlo, *Anal. Chem.*, 2014, **86**, 1502-1510.
85 D. R. Gossett, H. T. K. Tse, J. S. Dudani, K. Goda, T. A. Woods, S. W. Graves and D. Di Carlo, *Small*, 2012, **8**, 2757-2764.
86 C. M. Birch, H. W. Hou, J. Han and J. C. Niles, *Scientific reports*, 2015, **5**, 1-16.

87 M. S. Syed, M. Rafeie, D. Vandamme, M. Asadnia, R. Henderson, R. A. Taylor and M. E. Warkiani, *Bioresource technology*, 2018, **252**, 91-99.
88 M. Li, H. E. Muñoz, K. Goda and D. Di Carlo, *Scientific reports*, 2017, **7**, 1-8.
89 W. C. Lee, A. A. S. Bhagat, S. Huang, K. J. Van Vliet, J. Han and C. T. Lim, *Lab Chip*, 2011, **11**, 1359-1367.
90 E. W. Kemna, R. M. Schoeman, F. Wolbers, I. Vermes, D. A. Weitz and A. van den Berg, *Lab Chip*, 2012, **12**, 2881-2887.
91 D. Stoecklein and D. Di Carlo, *Anal. Chem.*, 2018, **91**, 296-314.
92 B. Ho and L. Leal, *Journal of Fluid Mechanics*, 1976, **76**, 783-799.
93 P. Huang, J. Feng, H. H. Hu and D. D. Joseph, *Journal of Fluid Mechanics*, 1997, **343**, 73-94.
94 X. Lu, C. Liu, G. Hu and X. Xuan, *J. Colloid Interface Sci.*, 2017, **500**, 182-201.
95 J. A. Pathak, D. Ross and K. B. Migler, *Phys. Fluids*, 2004, **16**, 4028-4034.
96 D. Yuan, Q. Zhao, S. Yan, S.-Y. Tang, Y. Zhang, G. Yun, N.-T. Nguyen, J. Zhang, M. Li and W. Li, *Lab Chip*, 2019, **19**, 2811-2821.
97 D. Yuan, J. Zhang, R. Sluyter, Q. Zhao, S. Yan, G. Alici and W. Li, *Lab on a Chip*, 2016, **16**, 3919-3928.
98 L. Rems, D. Kawale, L. J. Lee and P. E. Boukany, *Biomicrofluidics*, 2016, **10**, 043403.
99 K. Kang, S. S. Lee, K. Hyun, S. J. Lee and J. M. Kim, *Nat. Commun.*, 2013, **4**, Art No. 2567.
100 J. Y. Kim, S. W. Ahn, S. S. Lee and J. M. Kim, *Lab Chip*, 2012, **12**, 2807-2814.
101 S. J. Haward, A. Jaishankar, M. S. Oliveira, M. A. Alves and G. H. McKinley, *Biomicrofluidics*, 2013, **7**, 044108.
102 R. G. Larson, *Journal of Rheology*, 2005, **49**, 1-70.
103 D. F. James, *Annual Review of Fluid Mechanics*, 2009, **41**, 129-142.
104 L. E. Rodd, D. Lee, K. H. Ahn and J. J. Cooper-White, *Journal of non-Newtonian fluid mechanics*, 2010, **165**, 1189-1203.
105 G. D'Avino, F. Greco and P. L. Maffettone, *Annual Review of Fluid Mechanics*, 2017, **49**, 341-360.
106 H. Lim, J. Nam and S. Shin, *Microfluidics and nanofluidics*, 2014, **17**, 683-692.
107 S. Yang, J. Y. Kim, S. J. Lee, S. S. Lee and J. M. Kim, *Lab Chip*, 2011, **11**, 266-273.
108 B. Ha, J. Park, G. Destgeer, J. H. Jung and H. J. Sung, *Analytical chemistry*, 2016, **88**, 4205-4210.
109 D. Yuan, J. Zhang, S. Yan, G. Peng, Q. Zhao, G. Alici, H. Du and W. Li, *Electrophoresis*, 2016, **37**, 2147-2155.
110 J. Nam, H. Lim, D. Kim, H. Jung and S. Shin, *Lab Chip*, 2012, **12**, 1347-1354.
111 D. J. Lee, H. Brenner, J. R. Youn and Y. S. Song, *Scientific reports*, 2013, **3**, 1-8.
112 Y. B. Bae, H. K. Jang, T. H. Shin, G. Phukan, T. T. Tran, G. Lee, W. R. Hwang and J. M. Kim, *Lab on a Chip*, 2016, **16**, 96-103.
113 C. Liu, J. Guo, F. Tian, N. Yang, F. Yan, Y. Ding, J. Wei, G. Hu, G. Nie and J. Sun, *ACS Nano*, 2017, **11**, 6968-6976.
114 J. C. Contreras-Naranjo, H.-J. Wu and V. M. Ugaz, *Lab on a Chip*, 2017, **17**, 3558-3577.
115 K. Kang, S. S. Lee, K. Hyun, S. J. Lee and J. M. Kim, *Nature communications*, 2013, **4**, 1-8.
116 E. A. Kwizera, M. Sun, A. M. White, J. Li and X. He, *ACS Biomaterials Science & Engineering*, 2021.
117 X.-B. Wang, Y. Huang, F. Becker and P. Gascoyne, *Journal of Physics D: Applied Physics*, 1994, **27**, 1571.

118 F. Yang, Y. Zhang, X. Cui, Y. Fan, Y. Xue, H. Miao and G. Li, *Biotechnology journal*, 2019, **14**, 1800181.
119 M. Alshareef, N. Metrakos, E. Juarez Perez, F. Azer, F. Yang, X. Yang and G. Wang, *Biomicrofluidics*, 2013, **7**, 011803.
120 C. Zhang, K. Khoshmanesh, A. Mitchell and K. Kalantar-Zadeh, *Analytical and bioanalytical chemistry*, 2010, **396**, 401-420.
121 N.-V. Nguyen, T. Le Manh, T. S. Nguyen, V. T. Le and N. Van Hieu, *Journal of Science: Advanced Materials and Devices*, 2021, **6**, 11-18.
122 N. Abd Rahman, F. Ibrahim and B. Yafouz, *Sensors*, 2017, **17**, 449.
123 M. Li, W. Li, J. Zhang, G. Alici and W. Wen, *J. Phys. D: Appl. Phys.*, 2014, **47**, 063001.
124 R. Pethig, *Biomicrofluidics*, 2010, **4**, 022811.
125 M. Li and R. K. Anand, *Journal of the American Chemical Society*, 2017, **139**, 8950-8959.
126 Y. Jia, Y. Ren and H. Jiang, *Electrophoresis*, 2015, **36**, 1744-1753.
127 S. Y. Tang, J. Zhu, V. Sivan, B. Gol, R. Soffe, W. Zhang, A. Mitchell and K. Khoshmanesh, *Advanced Functional Materials*, 2015, **25**, 4445-4452.
128 M. Sun, P. Agarwal, S. Zhao, Y. Zhao, X. Lu and X. He, *Analytical chemistry*, 2016, **88**, 8264-8271.
129 C. Birch and J. P. Landers, *Micromachines*, 2017, **8**, 76.
130 Y. Yildizhan, N. Erdem, M. Islam, R. Martinez-Duarte and M. Elitas, *Sensors*, 2017, **17**, 2691.
131 N. A. M. Yunus and N. G. Green, *Journal of Physics: Conference Series*, 2008, **142**, 012068.
132 X. Hu, P. H. Bessette, J. Qian, C. D. Meinhart, P. S. Daugherty and H. T. Soh, *Proceedings of the national academy of sciences*, 2005, **102**, 15757-15761.
133 M. S. Pommer, Y. Zhang, N. Keerthi, D. Chen, J. A. Thomson, C. D. Meinhart and H. T. Soh, *Electrophoresis*, 2008, **29**, 1213-1218.
134 H. Li and R. Bashir, *Sensors and Actuators B: Chemical*, 2002, **86**, 215-221.
135 J. I. Martínez-López, H. Moncada-Hernández, J. L. Baylon-Cardiel, S. O. Martínez-Chapa, M. Rito-Palomares and B. H. Lapizco-Encinas, *Analytical and bioanalytical chemistry*, 2009, **394**, 293-302.
136 A. Nakano, F. Camacho-Alanis, T.-C. Chao and A. Ros, *Biomicrofluidics*, 2012, **6**, 034108.
137 J. Zhu and X. Xuan, *Biomicrofluidics*, 2011, **5**, 024111.
138 C. Church, J. Zhu, J. Nieto, G. Keten, E. Ibarra and X. Xuan, *Journal of Micromechanics and Microengineering*, 2010, **20**, 065011.
139 B. H. Lapizco-Encinas, *Electrophoresis*, 2019, **40**, 358-375.
140 B. Cardenas-Benitez, B. Jind, R. C. Gallo-Villanueva, S. O. Martinez-Chapa, B. H. Lapizco-Encinas and V. H. Perez-Gonzalez, *Analytical Chemistry*, 2020, **92**, 12871-12879.
141 P. V. Jones, A. F. DeMichele, L. Kemp and M. A. Hayes, *Analytical and bioanalytical chemistry*, 2014, **406**, 183-192.
142 P. V. Jones, G. L. Salmon and A. Ros, *Analytical chemistry*, 2017, **89**, 1531-1539.
143 P. Chen, D. Chen, S. Li, X. Ou and B.-F. Liu, *TrAC Trends in Analytical Chemistry*, 2019, **117**, 2-12.
144 E. Iswardy, T.-C. Tsai, I.-F. Cheng, T.-C. Ho, G. C. Perng and H.-C. Chang, *Biosensors and Bioelectronics*, 2017, **95**, 174-180.
145 M. Nakano, Z. Ding and J. Suehiro, *Japanese Journal of Applied Physics*, 2015, **55**, 017001.

146 D. Cai, M. Xiao, P. Xu, Y.-C. Xu and W. Du, *Lab on a Chip*, 2014, **14**, 3917-3924.
147 T. Yoon, H. S. Moon, J. W. Song, K. A. Hyun and H. I. Jung, *Cytometry Part A*, 2019, **95**, 1135-1144.
148 D.-H. Lee, X. Li, A. Jiang and A. P. Lee, *Biomicrofluidics*, 2018, **12**, 054104.
149 E. Du, M. Dao and S. Suresh, *Extreme Mechanics Letters*, 2014, **1**, 35-41.
150 S.-B. Huang, M.-H. Wu, Y.-H. Lin, C.-H. Hsieh, C.-L. Yang, H.-C. Lin, C.-P. Tseng and G.-B. Lee, *Lab Chip*, 2013, **13**, 1371-1383.
151 A. Khamenehfar, T. Beischlag, P. Russell, M. Ling, C. Nelson and P. Li, *Biomicrofluidics*, 2015, **9**, 064104.
152 N. Nam-Trung, *Microfluid Nanofluid*, 2012, **12**, 1-16.
153 K. Wang, W. Zhou, Z. Lin, F. Cai, F. Li, J. Wu, L. Meng, L. Niu and H. Zheng, *Sensors and Actuators B: Chemical*, 2018, **258**, 1174-1183.
154 M. Hejazian, W. Li and N.-T. Nguyen, *Lab Chip*, 2015, **15**, 959-970.
155 N.-T. Nguyen, *Microfluidics and nanofluidics*, 2012, **12**, 1-16.
156 S. Yaman, M. Anil-Inevi, E. Ozcivici and H. C. Tekin, *Frontiers in bioengineering and biotechnology*, 2018, **6**, 192.
157 W. Zhao, T. Zhu, R. Cheng, Y. Liu, J. He, H. Qiu, L. Wang, T. Nagy, T. D. Querec and E. R. Unger, *Advanced functional materials*, 2016, **26**, 3990-3998.
158 W.-T. Wu, A. B. Martin, A. Gandini, N. Aubry, M. Massoudi and J. F. Antaki, *Microfluidics and nanofluidics*, 2016, **20**, 41.
159 J. Nam, H. Huang, H. Lim, C. Lim and S. Shin, *Anal. Chem.*, 2013, **85**, 7316-7323.
160 N. Bhagwat, K. Dulmage, C. H. Pletcher, L. Wang, W. DeMuth, M. Sen, D. Balli, S. S. Yee, S. Sa and F. Tong, *Scientific reports*, 2018, **8**, 1-14.
161 J. H. Kang, S. Krause, H. Tobin, A. Mammoto, M. Kanapathipillai and D. E. Ingber, *Lab Chip*, 2012, **12**, 2175-2181.
162 B. Kwak, J. Lee, D. Lee, K. Lee, O. Kwon, S. Kang and Y. Kim, *Biosens. Bioelectron.*, 2017, **88**, 153-158.
163 F. Fachin, P. Spuhler, J. M. Martel-Foley, J. F. Edd, T. A. Barber, J. Walsh, M. Karabacak, V. Pai, M. Yu and K. Smith, *Scientific reports*, 2017, **7**, 1-11.
164 B. D. Plouffe, M. Mahalanabis, L. H. Lewis, C. M. Klapperich and S. K. Murthy, *Analytical chemistry*, 2012, **84**, 1336-1344.
165 H. G. Kye, B. S. Park, J. M. Lee, M. G. Song, H. G. Song, C. D. Ahrberg and B. G. Chung, *Scientific reports*, 2019, **9**, 1-10.
166 Z. Wang, R. Wu, Z. Wang and R. Ramanujan, *Scientific reports*, 2016, **6**, 1-10.
167 J.-J. Lee, K. J. Jeong, M. Hashimoto, A. H. Kwon, A. Rwei, S. A. Shankarappa, J. H. Tsui and D. S. Kohane, *Nano letters*, 2014, **14**, 1-5.
168 C. Park, J. Lee, Y. Kim, J. Kim, J. Lee and S. Park, *Journal of microbiological methods*, 2017, **132**, 128-133.
169 M. Anil-Inevi, S. Yaman, A. A. Yildiz, G. Mese, O. Yalcin-Ozuysal, H. C. Tekin and E. Ozcivici, *Scientific reports*, 2018, **8**, 1-10.
170 T. Sun, Q. Huang, Q. Shi, H. Wang, X. Liu, M. Seki, M. Nakajima and T. Fukuda, *Microfluidics and nanofluidics*, 2015, **19**, 1169-1180.
171 E. Turker and A. Arslan-Yildiz, *ACS Biomaterials Science & Engineering*, 2018, **4**, 787-799.
172 L. Ren, S. Yang, P. Zhang, Z. Qu, Z. Mao, P. H. Huang, Y. Chen, M. Wu, L. Wang and P. Li, *Small*, 2018, **14**, 1801996.
173 I. Leibacher, P. Reichert and J. Dual, *Lab on a Chip*, 2015, **15**, 2896-2905.

174 L. Y. Yeo and J. R. Friend, *Annual review of fluid mechanics*, 2014, **46**, 379-406.
175 Y. Xie, H. Bachman and T. J. Huang, *TrAC Trends in Analytical Chemistry*, 2019, **117**, 280-290.
176 H. Bruus, *Lab on a Chip*, 2012, **12**, 1014-1021.
177 A. Fornell, K. Cushing, J. Nilsson and M. Tenje, *Applied Physics Letters*, 2018, **112**, 063701.
178 Y. Xie, Z. Mao, H. Bachman, P. Li, P. Zhang, L. Ren, M. Wu and T. J. Huang, *Journal of biomechanical engineering*, 2020, **142**, 031005.
179 Y. Gao, M. Wu, Y. Lin and J. Xu, *Micromachines*, 2020, **11**, 921.
180 T. Yang, V. Vitali and P. Minzioni, *Microfluidics and Nanofluidics*, 2018, **22**, 1-12.
181 M. E. Piyasena, P. P. Austin Suthanthiraraj, R. W. Applegate Jr, A. M. Goumas, T. A. Woods, G. P. López and S. W. Graves, *Analytical chemistry*, 2012, **84**, 1831-1839.
182 P. Augustsson, J. T. Karlsen, H.-W. Su, H. Bruus and J. Voldman, *Nature communications*, 2016, **7**, 1-9.
183 A. Fornell, H. Pohlit, Q. Shi and M. Tenje, *Scientific Reports*, 2021, **11**, 1-9.
184 W. Cui, M. He, H. Zhang, Y. Yang and X. Duan, Bulk acoustic wave resonator integrated microfluidics for rapid and high efficience fluids mixing and bioparticle trapping, 2016.
185 I. Leibacher, P. Hahn and J. Dual, *Microfluidics and Nanofluidics*, 2015, **19**, 923-933.
186 C. Richard, A. Fakhfouri, M. Colditz, F. Striggow, R. Kronstein-Wiedemann, T. Tonn, M. Medina-Sánchez, O. G. Schmidt, T. Gemming and A. Winkler, *Lab on a Chip*, 2019, **19**, 4043-4051.
187 Y. Xie, J. Rufo, R. Zhong, J. Rich, P. Li, K. W. Leong and T. J. Huang, *ACS nano*, 2020, **14**, 16220-16240.
188 X. Ding, S.-C. S. Lin, B. Kiraly, H. Yue, S. Li, I.-K. Chiang, J. Shi, S. J. Benkovic and T. J. Huang, *Proceedings of the National Academy of Sciences*, 2012, **109**, 11105-11109.
189 S. J. Raymond, D. J. Collins, R. O'Rorke, M. Tayebi, Y. Ai and J. Williams, *Scientific reports*, 2020, **10**, 1-12.
190 T. Laurell, F. Petersson and A. Nilsson, *Chemical Society Reviews*, 2007, **36**, 492-506.
191 Y. Chen, M. Wu, L. Ren, J. Liu, P. H. Whitley, L. Wang and T. J. Huang, *Lab on a Chip*, 2016, **16**, 3466-3472.
192 P. Li, Z. Mao, Z. Peng, L. Zhou, Y. Chen, P.-H. Huang, C. I. Truica, J. J. Drabick, W. S. El-Deiry and M. Dao, *Proceedings of the National Academy of Sciences*, 2015, **112**, 4970-4975.
193 P. Dow, K. Kotz, S. Gruszka, J. Holder and J. Fiering, *Lab on a Chip*, 2018, **18**, 923-932.
194 P. Ohlsson, K. Petersson, P. Augustsson and T. Laurell, *Scientific reports*, 2018, **8**, 1-11.
195 M. Wu, Y. Ouyang, Z. Wang, R. Zhang, P.-H. Huang, C. Chen, H. Li, P. Li, D. Quinn and M. Dao, *Proceedings of the National Academy of Sciences*, 2017, **114**, 10584-10589.
196 M. Tayebi, D. Yang, D. J. Collins and Y. Ai, *Nano Letters*, 2021.
197 M. Wu, C. Chen, Z. Wang, H. Bachman, Y. Ouyang, P.-H. Huang, Y. Sadovsky and T. J. Huang, *Lab on a Chip*, 2019, **19**, 1174-1182.
198 J. Gai, R. Nosrati and A. Neild, *Lab on a Chip*, 2020, **20**, 4262-4272.
199 K. Xu, C. P. Clark, B. L. Poe, J. A. Lounsbury, J. Nilsson, T. Laurell and J. P. Landers, *Analytical chemistry*, 2019, **91**, 2186-2191.
200 N.-T. Nguyen, S. T. Wereley and S. A. M. Shaegh, *Fundamentals and applications of microfluidics*, Artech house, 2019.
201 H. Fallahi, J. Zhang, H.-P. Phan and N.-T. Nguyen, *Micromachines*, 2019, **10**, 830.
202 K. Yamamoto, N. Ota and Y. Tanaka, *Analytical Chemistry*, 2020, **93**, 332-349.

203 H. Amini, W. Lee and D. Di Carlo, *Lab Chip*, 2014, **14**, 2739-2761.
204 D. Kim, M. Sonker and A. Ros, *Analytical chemistry*, 2018, **91**, 277-295.
205 I. Giouroudi and G. Kokkinis, *Nanomaterials*, 2017, **7**, 171.
206 N. Pamme, *Lab Chip*, 2006, **6**, 24-38.
207 J. Friend and L. Y. Yeo, *Reviews of Modern Physics*, 2011, **83**, 647.
208 P. Li and T. J. Huang, *Analytical chemistry*, 2018, **91**, 757-767.
209 S. K. Ravula, D. W. Branch, C. D. James, R. J. Townsend, M. Hill, G. Kaduchak, M. Ward and I. Brener, *Sensors and Actuators B: Chemical*, 2008, **130**, 645-652.
210 B. Cetin, M. B. Özer, E. Çağatay and S. Büyükkocak, *Biomicrofluidics*, 2016, **10**, 014112.
211 J. D. Adams, P. Thévoz, H. Bruus and H. T. Soh, *Applied physics letters*, 2009, **95**, 254103.
212 U. Kim and H. T. Soh, *Lab on a Chip*, 2009, **9**, 2313-2318.
213 J. N. Krishnan, C. Kim, H. J. Park, J. Y. Kang, T. S. Kim and S. K. Kim, *Electrophoresis*, 2009, **30**, 1457-1463.
214 K. Mutafopulos, P. Spink, C. Lofstrom, P. Lu, H. Lu, J. Sharpe, T. Franke and D. Weitz, *Lab on a Chip*, 2019, **19**, 2435-2443.
215 E. Lin, L. Rivera-Báez, S. Fouladdel, H. J. Yoon, S. Guthrie, J. Wieger, Y. Deol, E. Keller, V. Sahai and D. M. Simeone, *Cell systems*, 2017, **5**, 295-304. e294.
216 D. Huang and N. Xiang, *Lab on a Chip*, 2021, **21**, 1409-1417.
217 F. Del Giudice, H. Madadi, M. M. Villone, G. D'Avino, A. M. Cusano, R. Vecchione, M. Ventre, P. L. Maffettone and P. A. Netti, *Lab Chip*, 2015, **15**, 1912-1922.
218 P. Li, M. Liang, X. Lu, J. J. M. Chow, C. J. Ramachandra and Y. Ai, *Analytical chemistry*, 2019, **91**, 15425-15435.
219 X. Lu and X. Xuan, *Analytical chemistry*, 2015, **87**, 11523-11530.
220 J.-S. Park and H.-I. Jung, *Anal. Chem.*, 2009, **81**, 8280-8288.
221 N. M. Karabacak, P. S. Spuhler, F. Fachin, E. J. Lim, V. Pai, E. Ozkumur, J. M. Martel, N. Kojic, K. Smith and P.-i. Chen, *Nat. Protoc.*, 2014, **9**, 694-710.
222 H. Ranchon, R. Malbec, V. Picot, A. Boutonnet, P. Terrapanich, P. Joseph, T. Leïchlé and A. Bancaud, *Lab Chip*, 2016, **16**, 1243-1253.
223 J. Zhang, S. Yan, D. Yuan, Q. Zhao, S. H. Tan, N.-T. Nguyen and W. Li, *Lab Chip*, 2016, **16**, 3947-3956.
224 M. J. Kim, D. J. Lee, J. R. Youn and Y. S. Song, *RSC Adv.*, 2016, **6**, 32090-32097.
225 B. Miller, M. Jimenez and H. Bridle, *Sci. Rep.*, 2016, **6**.
226 T. S. Sim, K. Kwon, J. C. Park, J.-G. Lee and H.-I. Jung, *Lab Chip*, 2011, **11**, 93-99.
227 A. Abdulla, W. Liu, A. Gholamipour-Shirazi, J. Sun and X. Ding, *Anal. Chem.*, 2018, **90**, 4397-4405.
228 X. Wang and I. Papautsky, *Lab Chip*, 2015, **15**, 1350-1359.
229 P. Sajeesh and A. K. Sen, *Microfluidics and nanofluidics*, 2014, **17**, 1-52.
230 H.-D. Xi, H. Zheng, W. Guo, A. M. Gañán-Calvo, Y. Ai, C.-W. Tsao, J. Zhou, W. Li, Y. Huang and N.-T. Nguyen, *Lab on a Chip*, 2017, **17**, 751-771.
231 M. Wiklund, C. Günther, R. Lemor, M. Jäger, G. Fuhr and H. M. Hertz, *Lab on a Chip*, 2006, **6**, 1537-1544.
232 D. J. Collins, T. Alan and A. Neild, *Lab Chip*, 2014, **14**, 1595-1603.
233 C. D. James, J. McClain, K. R. Pohl, N. Reuel, K. E. Achyuthan, C. J. Bourdon, K. Rahimian, P. C. Galambos, G. Ludwig and M. S. Derzon, *Journal of Micromechanics and Microengineering*, 2010, **20**, 045015.
234 Q. Chen, D. Li, J. Lin, M. Wang and X. Xuan, *Analytical chemistry*, 2017, **89**, 6915-6920.

235 M. Serhatlioglu, Z. Isiksacan, M. Özkan, D. n. s. Tuncel and C. Elbuken, *Analytical chemistry*, 2020, **92**, 6932-6940.
236 T. P. Hunt, D. Issadore and R. M. Westervelt, *Lab on a Chip*, 2008, **8**, 81-87.
237 D. Issadore, T. Franke, K. A. Brown, T. P. Hunt and R. M. Westervelt, *Journal of Microelectromechanical Systems*, 2009, **18**, 1220-1225.
238 V. Kumar and P. Rezai, *Biomedical microdevices*, 2017, **19**, 39.
239 S. Dibaji and P. Rezai, *Journal of Magnetism and Magnetic Materials*, 2020, **503**, 166620.
240 P. G. Saffman, *J. Fluid Mech.*, 1965, **22**, 385-400.
241 J. Zhang, S. Yan, D. Yuan, G. Alici, N.-T. Nguyen, M. Ebrahimi Warkiani and W. Li, *Lab Chip*, 2016, **16**, 10-34.
242 Y. W. Kim and J. Y. Yoo, *Lab Chip*, 2009, **9**, 1043-1045.
243 A. S. Khair and J. K. Kabarowski, *Physical Review Fluids*, 2020, **5**, 033702.
244 D. Yuan, C. Pan, J. Zhang, S. Yan, Q. Zhao, G. Alici and W. Li, *Micromachines*, 2016, **7**, 195.
245 D. Li and X. Xuan, *Physical Review Fluids*, 2018, **3**, 074202.
246 V. Lochab and S. Prakash, *Soft Matter*, 2021, **17**, 611-620.
247 A. Choudhary, T. Renganathan and S. Pushpavanam, *J. Fluid Mech.*, 2019, **874**, 856-890.
248 C. Prohm, F. Tröltzsch and H. Stark, *The European Physical Journal E*, 2013, **36**, 1-13.
249 C. Prohm and H. Stark, *Lab Chip*, 2014, **14**, 2115-2123.
250 F. Rühle, C. Schaaf and H. Stark, *Micromachines*, 2020, **11**, 592.
251 A. Choudhary, D. Li, T. Renganathan, X. Xuan and S. Pushpavanam, *Journal of Fluid Mechanics*, 2020, **898**.
252 K. W. Seo, Y. J. Kang and S. J. Lee, *Physics of Fluids (1994-present)*, 2014, **26**, 063301.
253 G. Holzner, S. Stavrakis and A. DeMello, *Analytical chemistry*, 2017, **89**, 11653-11663.
254 E. J. Lim, T. J. Ober, J. F. Edd, S. P. Desai, D. Neal, K. W. Bong, P. S. Doyle, G. H. McKinley and M. Toner, *Nature communications*, 2014, **5**, 1-9.
255 Y. Zhou, Z. Ma and Y. Ai, *Lab Chip*, 2020, **20**, 568-581.
256 D. Yuan, S. H. Tan, Q. Zhao, S. Yan, R. Sluyter, N. T. Nguyen, J. Zhang and W. Li, *RSC Adv.*, 2017, **7**, 3461-3469.
257 D. Yuan, S. Yan, J. Zhang, R. M. Guijt, Q. Zhao and W. Li, *Anal. Chem.*, 2021, **93**, 12648-12654.
258 J. D. Adams, U. Kim and H. T. Soh, *Proc. Natl. Acad. Sci. U.S.A.*, 2008, **105**, 18165-18170.
259 C. Derec, C. Wilhelm, J. Servais and J.-C. Bacri, *Microfluid. Nanofluid.*, 2010, **8**, 123.
260 A. Kasukurti, C. Eggleton, S. Desai, D. Disharoon and D. Marr, *Lab on a Chip*, 2014, **14**, 4673-4679.
261 T. Luo, L. Fan, Y. Zeng, Y. Liu, S. Chen, Q. Tan, R. H. Lam and D. Sun, *Lab on a Chip*, 2018, **18**, 1521-1532.
262 C.-T. Huang, C.-H. Weng and C.-P. Jen, *Biomicrofluidics*, 2011, **5**, 044101.
263 K. Zhao, Larasati, B. P. Duncker and D. Li, *Analytical chemistry*, 2019, **91**, 6304-6314.
264 A. Shamloo and M. Boodaghi, *Ultrasonics*, 2018, **84**, 234-243.
265 M. G. Lee, S. Choi and J.-K. Park, *Journal of Chromatography A*, 2011, **1218**, 4138-4143.